Probing for chiral Z' gauge boson through scattering measurement experiments

Kento Asai,[1,*] Arindam Das,[2,3,†] Jinmian Li,[4,‡] Takaaki Nomura,[4,§] and Osamu Seto[3,‖]

[1]*Institute for Cosmic Ray Research (ICRR), The University of Tokyo, Kashiwa, Chiba 277-8582, Japan*
[2]*Institute for the Advancement of Higher Education, Hokkaido University, Sapporo 060-0817, Japan*
[3]*Department of Physics, Hokkaido University, Sapporo 060-0810, Japan*
[4]*College of Physics, Sichuan University, Chengdu 610065, China*

(Received 28 July 2023; accepted 3 February 2024; published 15 April 2024)

Motivated by the observation that tiny neutrino mass cannot be explained within the framework of the Standard Model, we consider extra gauge extended scenarios in which tiny neutrino masses are generated through the seesaw mechanism. These scenarios are equipped with a beyond the Standard Model neutral gauge boson called Z' in the general $U(1)_X$ symmetry, which is a linear combination of $U(1)_Y$ and $U(1)_{B-L}$. In this case, left- and right-handed fermions interact differently with the Z'. The Z' gives rise to different processes involving neutrino-nucleon, neutrino-electron, electron-nucleus, and electron-muon scattering processes. By comparing with proton and electron beam-dump experiment data, recast data from searches for the long-lived and dark photon at *BABAR*, LHCb, and CMS experiments, the electron and muon $g-2$ data, and the data of the dilepton and dijet searches at the LEP experiment, we derive bounds on the gauge coupling and the corresponding gauge boson mass for different $U(1)_X$ charges and evaluate the prospective limits from the future beam-dump scenarios at DUNE, FASER (2), and ILC. We conclude that large parameter regions could be probed by scattering, beam-dump, and collider experiments in the future.

DOI: 10.1103/PhysRevD.109.075026

I. INTRODUCTION

Tiny neutrino masses and flavor mixing are important experimental observations [1] that motivate us to think beyond the Standard Model (SM). Various cosmological data indicate that nonluminous objects, called dark matter, capture nearly 0.25 fraction of the energy budget of the Universe [2,3], which further indicate that an extension of the SM is certain. The origin of tiny neutrino mass can be explained by the seesaw mechanism, where the SM is extended by SM-singlet Majorana right-handed neutrinos (RHNs) [4–8]. In this case, light neutrino mass can be originated by the suppression of the heavy mass scale of the RHNs, which introduces a lepton number violation of unit two, which is a nice realization of the dimension-five Weinberg operator [9].

This simple but interesting ultraviolet (UV) theory is constructed if the SM is extended by a general $U(1)_X$ gauge group that is a linear combination of $U(1)_Y$ and $U(1)_{B-L}$. In this setup, three generations of SM-singlet RHNs are introduced to cancel the gauge and mixed gauge-gravity anomalies. After the general $U(1)_X$ symmetry is broken by a SM-singlet scalar, the scalar acquires the vacuum expectation value (VEV), which lets the RHNs acquire Majorana masses. Followed by the electroweak symmetry breaking, a Dirac mass term is generated from the Yukawa interaction between the SM lepton and Higgs doublets along with the SM-singlet RHNs. These Majorana and Dirac masses get involved in the seesaw mechanism to generate light neutrino mass and flavor mixing [10]. All these couplings and interactions are protected by general $U(1)_X$ gauge symmetry.

In general, an extra gauged $U(1)$ extension of the SM, a neutral and beyond the SM (BSM) gauge boson, commonly known as the Z', exists and acquires the mass after the extra $U(1)$ symmetry breaking. New physics contributions from the Z' are considered to be very well motivated and are being studied at low- and high-energy experiments [11–43] from various aspects. A remarkable aspect of our general $U(1)_X$ models compared with the others studied previously is that the SM left and right chiral fermions could be charged differently under the $U(1)_X$. We will study such a chiral scenario to estimate the limits on the general $U(1)_X$

*kento@icrr.u-tokyo.ac.jp
†arindamdas@oia.hokudai.ac.jp
‡jmli@scu.edu.cn
§nomura@scu.edu.cn
‖seto@particle.sci.hokudai.ac.jp

gauge coupling with respect to the Z' mass for different general $U(1)_X$ charges and compare with a variety of existing bounds for the Z' mass to be probed. In this paper, we consider two cases of general $U(1)_X$ extensions of the SM. Those two are solutions of anomaly-free conditions and mathematically equally possible. In the first case, three generations of RHNs are universal under the general $U(1)_X$ gauge group having the same charge. The second is another less-studied, interesting possibility where the first two generations of the RHNs have general $U(1)_X$ charge -4, the third generation RHN has the charge $+5$, and two $SU(2)_L$ Higgs doublets are differently charged under the general $U(1)_X$ gauge group. One of the $SU(2)_L$ Higgs doublets couples with the RHNs and charged leptons, which makes the scenario neutrinophilic. In addition to the doublet scalars, we introduce three SM-singlet scalars that are differently charged under the general $U(1)_X$ gauge group. We call the second case an alternative general $U(1)_X$ scenario. Because of the anomaly cancellation conditions, left- and right-handed SM fermions must be differently charged under the general $U(1)_X$ gauge group manifesting the chiral nature of the model.

We study the chiral nature of the Z' interactions through the Z' mediated neutrino-electron, neutrino-nucleon, and electron-muon scattering processes at different experiments such as FASERν and FASERν2 [44–51], SND@LHC [52–55], NA64 [56–61], JSNS2, COHERENT, and MUonE [62,63]. These are the Z' mediated t-channel processes and those interaction vertices depending on general $U(1)_X$ charges manifest the chiral nature, which has not been studied before in the literature for these experiments.

In order to compare our results with the existing bounds, we obtain respective bounds from different scattering and beam-dump experiments in the chiral scenario. To do that, we estimate bounds from the electron/positron beam-dump experiments Orsay [64], NA64 [65], KEK [66], E141 [67], E137 [68], and E774 [69]. Studying the bounds from the neutrino-electron scattering experiments from TEXONO [70–72], BOREXINO [73–78], and JSNS2 at the J-PARC experiment [79], we compare our results for different $U(1)_X$ charges. Depending on the choice of the Z' mass, we compare our bounds for muon neutrino- and muon antineutrino-electron scattering from the CHARM-II experiment [80–83]. We study neutrino-nucleon scattering to estimate bounds for different $U(1)_X$ charges from the COHERENT experiment [84–88]. In addition to those, we compare our results with the GEMMA experiment studying neutrino magnetic moments [27,89]. We compare the bounds from the dark photon searches at the LHCb experiment [14,25], dark photon searches from the CMS experiment [90], and visible and invisible decay of dark photons from the *BABAR* experiment [91,92]. We compare our results with proton beam-dump experiments like NOMAD [93], CHARM [94], and ν-cal [95,96] experiments. We compare our bounds with the dilepton and dijet final states from the LEP-II study [97–100]. Finally, we estimate bounds on general $U(1)_X$ coupling with respect to $M_{Z'}$ from muon and electron $g-2$ experiments to show the complementarity scenario.

Our paper is organized as follows. We discuss the models in Sec. II. We calculate constraints on the gauge coupling for different $U(1)_X$ charges in Sec. III. We discuss our results in Sec. IV and finally conclude the paper in Sec. V.

II. MODEL

A general $U(1)_X$ extension of the SM involves three generations of RHNs to cancel the gauge and mixed gauge-gravity anomalies. As a result, we observe that left- and right-handed charged fermions in the SM are differently charged under the $U(1)$ group. We write down the UV-complete models in the following.

A. Case I

We consider a general $U(1)_X$ extension of the SM to investigate the chiral scenario introducing three RHNs (N_R) and an SM-singlet scalar (Φ) field. Three generations of RHNs are introduced to cancel gauge and mixed gauge-gravity anomalies. The corresponding field content is given in Table I where general $U(1)_X$ charges, being independent of generations, are written as $\tilde{x}_f$ before anomaly cancellation and f stands for the three generations of quarks $(q_L^\alpha, u_R^\alpha, d_R^\alpha)$ and leptons $(\ell_L^\alpha, e_R^\alpha, N_R^\alpha)$, respectively, where $\alpha(=1,2,3)$ is the generation index. The gauge and mixed gauge-gravity anomaly cancellation conditions in terms of the general charges are written as follows:

$$\begin{aligned}
&\mathrm{U}(1)_X \otimes [SU(3)_C]^2 : 2\tilde{x}_q - \tilde{x}_u - \tilde{x}_d = 0,\\
&\mathrm{U}(1)_X \otimes [SU(2)_L]^2 : 3\tilde{x}_q + \tilde{x}_\ell = 0,\\
&\mathrm{U}(1)_X \otimes [\mathrm{U}(1)_Y]^2 : \tilde{x}_q - 8\tilde{x}_u - 2\tilde{x}_d + 3\tilde{x}_\ell - 6\tilde{x}_e = 0,\\
&[\mathrm{U}(1)_X]^2 \otimes \mathrm{U}(1)_Y : \tilde{x}_q^2 - 2\tilde{x}_u^2 + \tilde{x}_d^2 - \tilde{x}_\ell^2 + \tilde{x}_e{}^2 = 0,\\
&[\mathrm{U}(1)_X]^3 : 6\tilde{x}_q{}^3 - 3\tilde{x}_u{}^3 - 3\tilde{x}_d{}^3 + 2\tilde{x}_\ell{}^3 - \tilde{x}_\nu^3 - \tilde{x}_e^3 = 0,\\
&\mathrm{U}(1)_X \otimes [\mathrm{grav}]^2 : 6\tilde{x}_q - 3\tilde{x}_u - 3\tilde{x}_d + 2\tilde{x}_\ell - \tilde{x}_\nu - \tilde{x}_e = 0.
\end{aligned} \tag{1}$$

The Yukawa interactions between the fermions and the scalars (H, Φ) can be written following the $\mathcal{G}_{\mathrm{SM}} \otimes U(1)_X$ gauge symmetry as

$$\begin{aligned}
\mathcal{L}^{\mathrm{Yukawa}} = &-Y_u^{\alpha\beta}\overline{q_L^\alpha} H u_R^\beta - Y_d^{\alpha\beta}\overline{q_L^\alpha}\,\tilde{H}\, d_R^\beta - Y_e^{\alpha\beta}\overline{\ell_L^\alpha}\,\tilde{H}\, e_R^\beta\\
&- Y_\nu^{\alpha\beta}\overline{\ell_L^\alpha} H N_R^\beta - Y_N^\alpha \Phi \overline{(N_R^\alpha)^c} N_R^\alpha + \mathrm{H.c.},
\end{aligned} \tag{2}$$

where H is the SM Higgs doublet and we transform it into $\tilde{H}$ following $i\tau^2 H^*$ where τ^2 is the second Pauli matrix. Hence, using Eq. (2) and following charge neutrality, we

TABLE I. Field content of general $U(1)_X$ extension of the SM in the minimal form with the charges of the particles before and after anomaly cancellation considering different benchmark values of x_H setting $x_\Phi = 1$. In this charge assignment, $x_H = 0$ and -2 are the $U(1)_{B-L}$ and $U(1)_{\rm R}$ scenarios. Among the chiral scenarios, $U(1)_{B-L}$ is a vectorlike case.

	$SU(3)_C$	$SU(3)_L$	$U(3)_Y$	$U(1)_X$	-2 $U(1)_{\rm R}$	-1	-0.5	0 $U(1)_{B-L}$	0.5	1	2
q_L^α	**3**	**2**	$\frac{1}{6}$	$\tilde{x}_q = \frac{1}{6}x_H + \frac{1}{3}x_\Phi$	0	$\frac{1}{6}$	$\frac{1}{4}$	$\frac{1}{3}$	$\frac{5}{12}$	$\frac{1}{2}$	$\frac{1}{3}$
u_R^α	**3**	**1**	$\frac{2}{3}$	$\tilde{x}_u = \frac{2}{3}x_H + \frac{1}{3}x_\Phi$	-1	$-\frac{1}{3}$	0	$\frac{1}{3}$	$\frac{1}{2}$	1	$\frac{5}{3}$
d_R^α	**3**	**1**	$-\frac{1}{3}$	$\tilde{x}_d = -\frac{1}{3}x_H + \frac{1}{3}x_\Phi$	1	$\frac{2}{3}$	$\frac{1}{2}$	$\frac{1}{3}$	$\frac{1}{6}$	0	$-\frac{1}{3}$
ℓ_L^α	**1**	**2**	$-\frac{1}{2}$	$\tilde{x}_\ell = -\frac{1}{2}x_H - x_\Phi$	0	$-\frac{1}{2}$	$-\frac{3}{4}$	-1	$\frac{5}{4}$	$-\frac{3}{2}$	-2
e_R^α	**1**	**1**	-1	$\tilde{x}_e = -x_H - x_\Phi$	1	0	$-\frac{1}{2}$	-1	$-\frac{3}{2}$	-2	-3
N_R^α	**1**	**1**	0	$\tilde{x}_\nu = -x_\Phi$	-1	-1	-1	-1	-1	-1	-1
H	**1**	**2**	$-\frac{1}{2}$	$\tilde{x}_H = -\frac{1}{2}x_H$	1	$\frac{1}{2}$	$\frac{1}{4}$	0	$-\frac{1}{4}$	$-\frac{1}{2}$	-1
Φ	**1**	**1**	0	$\tilde{x}_\Phi = 2x_\Phi$	2	2	2	2	2	2	2

express the following relations between the general $U(1)_X$ charges of the particles as

$$-\frac{1}{2}x_H = -\tilde{x}_q + \tilde{x}_u = \tilde{x}_q - \tilde{x}_d = \tilde{x}_\ell - \tilde{x}_e = -\tilde{x}_\ell + \tilde{x}_\nu,$$
$$2x_\Phi = -2\tilde{x}_\nu. \tag{3}$$

The general $U(1)_X$ charges of the fermions can be obtained solving Eqs. (1) and (3) which finally can be expressed using the scalar charges x_H and x_Φ, respectively. Simply, the anomaly-free charge assignment of the general $U(1)_X$ can be expressed in terms of a linear combination of two anomaly-free scenarios, namely, $U(1)_Y$ of the SM and $B-L$ charges. Finally, we find that the left- and right-handed fermions under the general $U(1)_X$ scenario have different charges and hence they interact differently with the neutral BSM gauge boson Z' in the model. We take $x_\Phi = 1$ without the loss of generality, which corresponds to the $U(1)_{B-L}$ and $U(1)_R$ scenarios with $x_H = 0$ [101–106] and $x_H = 2$ [107–111], respectively. $U(1)_{B-L}$ is a vectorlike scenario where left- and right-handed fermions of the same type are equally charged under the $U(1)$ extension. In the case of the $U(1)_R$ scenario, we find that left-handed fermions do not interact with the Z'. Using the general form of the $U(1)$ charges of the charged fermions, we notice that for $x_H = -1$ the $U(1)$ charge of the right-handed electron (e_R) becomes zero and, as a result, it has no direct interaction with the Z', whereas other fermions will interact with the Z', manifesting the chiral nature of the model. In a similar fashion, we find that for $x_H = -0.5$ the general $U(1)_X$ charge of the right-handed up-type quark u_R is zero, implying no direct interaction with the Z', whereas other fermions will have nonzero general $U(1)_X$ charges, allowing direct interactions with the Z'. Similar behavior could be observed when $x_H = 1$, where the general $U(1)_X$ charge of the right-handed down-type quark (d_R) is zero. resulting in no direct interaction with the Z'. Detailed charge assignments for these combinations of x_H and x_Φ are given in Table I. We consider two more scenarios with $x_H = 0.5$ and 2, setting $x_\Phi = 1$, where all the charged fermions interact with the Z', manifesting the chiral behavior of the model.

The scalar sector of this scenario can be explored by introducing the renormalizable potential of this model, which can be given by

$$V = m_H^2(H^\dagger H) + \lambda_H(H^\dagger H)^2 + m_\Phi^2(\Phi^\dagger\Phi) + \lambda_\Phi(\Phi^\dagger\Phi)^2 + \lambda_{\rm mix}(H^\dagger H)(\Phi^\dagger\Phi), \tag{4}$$

where H and Φ can be separately approximated in the analysis of scalar potential, by taking $\lambda_{\rm mix}$ to be very small. After the breaking of general $U(1)_X$ and electroweak symmetries, the scalar fields develop VEVs as follows:

$$\langle H\rangle = \frac{1}{\sqrt{2}}\begin{pmatrix} v \\ 0 \end{pmatrix} \quad \text{and} \quad \langle\Phi\rangle = \frac{v_\Phi}{\sqrt{2}}, \tag{5}$$

where $v = 246$ GeV is marked as the electroweak scale VEV at the potential minimum and v_Φ is a free parameter. After the general $U(1)_X$ symmetry is broken, the mass of the BSM neutral gauge boson can be evolved setting $x_\Phi = 1$ as

$$M_{Z'} = 2g_X v_\Phi, \tag{6}$$

in the limit of $v_\Phi \gg v$. Here, g_X is the general $U(1)_X$ coupling and the Z' mass is a free parameter.

B. Case II

We consider another scenario where the SM is extended by a general $U(1)_X$ gauge group with three generations of RHNs. The field content of the model is given in Table II. The general U(1) charges of the charged fermion fields are the same for all generations, $\alpha(=1,2,3)$ where α is the generation index. The general $U(1)_X$ charges of the fields are written as $\tilde{x}_f$ before anomaly cancellation and f stands for the three generations of quarks $(q_L^\alpha, u_R^\alpha, d_R^\alpha)$ and

TABLE II. Field content of the general $U(1)_X$ extension of the SM in the minimal form with the charges of the particles before and after anomaly cancellation considering different benchmark values of x_H. Here, $x_H = 0$ is an alternative $B-L$ case, which is purely vectorlike structure given as a reference in this article.

	$SU(3)_C$	$SU(2)_L$	$U(1)_Y$	$U(1)_X$	-2 $U(1)_R$	-1	-0.5	0 $B-L$	0.5	1	2
q_L^α	**3**	**2**	$\frac{1}{6}$	$\tilde{x}_q = \frac{1}{6}x_H + \frac{1}{3}$	0	$\frac{1}{6}$	$\frac{1}{4}$	$\frac{1}{3}$	$\frac{5}{12}$	$\frac{1}{2}$	$\frac{1}{3}$
u_R^α	**3**	**1**	$\frac{2}{3}$	$\tilde{x}_u = \frac{2}{3}x_H + \frac{1}{3}$	-1	$-\frac{1}{3}$	0	$\frac{1}{3}$	$\frac{1}{2}$	1	$\frac{5}{3}$
d_R^α	**3**	**1**	$-\frac{1}{3}$	$\tilde{x}_d = -\frac{1}{3}x_H + \frac{1}{3}$	1	$\frac{2}{3}$	$\frac{1}{2}$	$\frac{1}{3}$	$\frac{1}{6}$	0	$-\frac{1}{3}$
ℓ_L^α	**1**	**2**	$-\frac{1}{2}$	$\tilde{x}_\ell = -\frac{1}{2}x_H - 1$	0	$-\frac{1}{2}$	$-\frac{3}{4}$	-1	$\frac{5}{4}$	$-\frac{3}{2}$	-2
e_R^α	**1**	**1**	-1	$\tilde{x}_e = -x_H - 1$	1	0	$-\frac{1}{2}$	-1	$-\frac{3}{2}$	-2	-3
$N_R^{1,2}$	**1**	**1**	0	$\tilde{x}_\nu = -4$	-4	-4	-4	-4	-4	-4	-4
N_R^3	**1**	**1**	0	$\tilde{x}'_\nu = 5$	5	5	5	5	5	5	5
H_1	**1**	**2**	$-\frac{1}{2}$	$\tilde{x}_{H_1} = -\frac{x_H}{2}$	1	$\frac{1}{2}$	$\frac{1}{4}$	0	$-\frac{1}{4}$	$-\frac{1}{2}$	-1
H_2	**1**	**2**	$-\frac{1}{2}$	$\tilde{x}_{H_2} = -\frac{1}{2}x_H + 3$	4	$\frac{7}{2}$	$\frac{13}{2}$	3	$\frac{11}{4}$	$\frac{5}{2}$	2
Φ_1	**1**	**1**	0	$\tilde{x}_{\Phi_1} = +8$	$+8$	$+8$	$+8$	$+8$	$+8$	$+8$	$+8$
Φ_2	**1**	**1**	0	$\tilde{x}_{\Phi_2} = -10$	-10	-10	-10	-10	-10	-10	-10
Φ_3	**1**	**1**	0	$\tilde{x}_{\Phi_3} = -3$	-3	-3	-3	-3	-3	-3	-3

leptons $(\ell_L^\alpha, e_R^\alpha)$. We introduce two $SU(2)$ doublet Higgs fields $(H_{1,2})$, where one is SM-like (H_1) and the other one is the BSM (H_2) Higgs. Because of different general $U(1)_X$ charge assignments, H_1 does not couple with the BSM fermions. We introduce three SM-singlet scalar fields $(\Phi_{1,2,3})$ that are differently charged under the general $U(1)_X$ gauge group. Because of the general $U(1)_X$ gauge symmetry, the first two generations of the RHNs have charge -4 each and the third generation RHN has $+5$ charge under the general $U(1)_X$ gauge group [112]. The RHNs with semi-non-universal $U(1)$ charges in this model help to cancel gauge and mixed gauge-gravity anomalies. As a result, we call this model an alternative general $U(1)_X$ scenario. Following the gauge and mixed gauge-gravity anomaly cancellation conditions, we relate the general $U(1)_X$ charges of the charged fermions as

$$\begin{aligned}
U(1)_X \otimes [SU(3)_C]^2&: \ 2\tilde{x}_q - \tilde{x}_u - \tilde{x}_d = 0,\\
U(1)_X \otimes [SU(2)_L]^2&: \ 3\tilde{x}_q + \tilde{x}_\ell = 0,\\
U(1)_X \otimes [U(1)_Y]^2&: \ \tilde{x}_q - 8\tilde{x}_u - 2\tilde{x}_d + 3\widetilde{x_\ell} - 6\widetilde{x_e} = 0,\\
[U(1)_X]^2 \otimes U(1)_Y&: \ \tilde{x}_q^2 - 2\tilde{x}_u{}^2 + \tilde{x}_d^2 - \tilde{x}_\ell^2 + \tilde{x}_e^2 = 0,\\
[U(1)_X]^3&: \ 3(6\tilde{x}_q{}^3 - 3\tilde{x}_u{}^3 - 3\tilde{x}_d{}^3 + 2\tilde{x}_\ell{}^3 - \tilde{x}_e^3)\\
&\quad - 2\tilde{x}_\nu^3 - \tilde{x}_\nu^{\prime 3} = 0,\\
U(1)_X \otimes [\mathrm{grav}]^2&: \ 3(6\tilde{x}_q - 3\tilde{x}_u - 3\tilde{x}_d + 2\tilde{x}_\ell - \tilde{x}_e)\\
&\quad - 2\tilde{x}_\nu - \tilde{x}'_\nu = 0.
\end{aligned} \tag{7}$$

We find that due to general $U(1)_X$ charges the SM charged fermions interact differently with the Z', manifesting the chiral nature of the model. The second Higgs doublet H_2 interacts with the SM lepton doublet (ℓ_L^α) and the first two generations of the RHNs $(N_R^{1,2})$ due to the general $U(1)_X$ symmetry. Hence, the Dirac Yukawa mass term for $N_R^{1,2}$ can be generated. On the other hand, the corresponding Majorana mass term for $N_R^{1,2}$ can be generated from the Dirac Yukawa coupling with Φ_1 followed by the general $U(1)_X$ symmetry breaking. The third generation of the RHN, N_R^3, has no Dirac Yukawa coupling involving any of the doublet Higgs fields being prohibited by the general $U(1)_X$ charge assignments. Therefore, it does not participate in the neutrino mass generation mechanism at the tree level; however, it can have Yukawa interaction with the Φ_2, which further generates a Majorana mass term for N_R^3 after the general $U(1)_X$ symmetry breaking. Finally, we write the Yukawa interaction among the BSM sector as

$$\begin{aligned}
-\mathcal{L}_{\mathrm{int}} \supset &\sum_{\alpha=1}^{3}\sum_{\beta=1}^{2} Y_1^{\alpha\beta}\overline{\ell_L^\alpha} H_2 N_R^\beta + \frac{1}{2}\sum_{\alpha=1}^{2} Y_2^\alpha \Phi_1 \overline{(N_R^\alpha)^c} N_R^\alpha\\
&+ \frac{1}{2} Y_3 \Phi_2 \overline{(N_R^3)^c} N_R^3 + \mathrm{H.c.},
\end{aligned} \tag{8}$$

taking Y_2 as being diagonal without the loss of generality. As in the previous case, we can solve the gauge and mixed gauge-gravity anomalies to estimate the charges of the SM particles in Table II.

The scalar potential of this scenario can be given by

$$
\begin{aligned}
V = {} & m_{H_1}^2(H_1^\dagger H_1) + \lambda_{H_1}(H_1^\dagger H_1)^2 + m_{H_2}^2(H_2^\dagger H_2) + \lambda_{H_2}(H_2^\dagger H_2)^2 \\
& + m_{\Phi_1}^2(\Phi_1^\dagger \Phi_1) + \lambda_1(\Phi_1^\dagger \Phi_1)^2 + m_{\Phi_2}^2(\Phi_2^\dagger \Phi_2) + \lambda_2(\Phi_2^\dagger \Phi_2)^2 \\
& + m_{\Phi_3}^2(\Phi_3^\dagger \Phi_3) + \lambda_3(\Phi_3^\dagger \Phi_3)^2 + (\mu \Phi_3(H_1^\dagger H_2) + \text{H.c.}) \\
& + \lambda_4(H_1^\dagger H_1)(H_2^\dagger H_2) + \lambda_5(H_1^\dagger H_2)(H_2^\dagger H_1) + \lambda_6(H_1^\dagger H_1)(\Phi_1^\dagger \Phi_1) \\
& + \lambda_7(H_1^\dagger H_1)(\Phi_2^\dagger \Phi_2) + \lambda_8(H_1^\dagger H_2)(\Phi_3^\dagger \Phi_3) + \lambda_9(H_2^\dagger H_2)(\Phi_1^\dagger \Phi_1) \\
& + \lambda_{10}(H_1^\dagger H_1)(\Phi_2^\dagger \Phi_2) + \lambda_{11}(H_1^\dagger H_2)(\Phi_3^\dagger \Phi_3) + \lambda_{12}(\Phi_1^\dagger \Phi_1)(\Phi_2^\dagger \Phi_2) \\
& + \lambda_{13}(\Phi_2^\dagger \Phi_2)(\Phi_3^\dagger \Phi_3) + \lambda_{14}(\Phi_3^\dagger \Phi_3)(\Phi_1^\dagger \Phi_1). \qquad (9)
\end{aligned}
$$

Choosing suitable parametrization for the scalar fields in this scenario to develop their respective VEVs, we can write

$$
\langle H_1 \rangle = \frac{1}{\sqrt{2}} \begin{pmatrix} v_{h_1} \\ 0 \end{pmatrix}, \qquad \langle H_2 \rangle = \frac{1}{\sqrt{2}} \begin{pmatrix} v_{h_2} \\ 0 \end{pmatrix}, \qquad \langle \Phi_1 \rangle = \frac{v_1}{\sqrt{2}}, \qquad \langle \Phi_2 \rangle = \frac{v_2}{\sqrt{2}}, \qquad \langle \Phi_3 \rangle = \frac{v_3}{\sqrt{2}}, \qquad (10)
$$

with the condition, $\sqrt{v_{h_1}^2 + v_{h_2}^2} = 246$ GeV. In this alternative general $U(1)_X$ extension of the SM, we consider negligibly small scalar quartic couplings among SM scalar doublet fields $H_{1,2}$ and SM-singlet scalar fields $\Phi_{1,2,3}$. As a result, this ensures higher-order mixing between the RHNs after the general $U(1)_X$ breaking to be very strongly suppressed. In Eq. (9), we may consider $0 < m_{\text{mix}}^2 = \mu v_3/\sqrt{2} \ll m_{\Phi_3}^2$, which further leads to $v_{h_2} \sim m_{\text{mix}}^2 v_{h_1}/m_{\Phi_3}^2 \ll v_{h_1}$ [113].

Because of the presence of the general $U(1)_X$ gauge symmetry, the doublet scalar sector $H_{1,2}$ and singlet scalar sector $\Phi_{1,2,3}$ interact only through the coupling $\Phi_3(H_1^\dagger H_2) + \text{H.c.}$; however, this coupling has no significant effect to determine the VEVs $(v_{1,2,3})$ of the singlet scalar fields $(\Phi_{1,2,3})$ because there is already one collider constraint present in the form of $v_1^2 + v_2^2 + v_3^2 \gg v_{h_1}^2 + v_{h_2}^2$. One finds that $\sqrt{v_1^2 + v_2^2 + v_3^2}$ should be typically larger than around 1 TeV from various constraints in the light Z' case [11] and the constraint from dilepton resonance in the heavy Z' case [114,115], since the value is related to the Z' boson mass and new gauge coupling. Therefore, we arrange the parameters of the scalar potential in a way so that the VEVs of $\Phi_{1,2,3}$ will be almost the same following $\mu < v_1$, whereas Φ_3 can be considered as a spurion field that generates the mixing between $H_{1,2}$ in Eq. (9). Once the Φ_3 acquires the VEV, we get the mixing mass term between $H_{1,2}$ as $m_{\text{mix}} = \frac{\mu v_3}{\sqrt{2}}$, which resembles the potential of the two Higgs doublet model; however, due to the presence of the general $U(1)_X$ symmetry, the SM-singlet fields $\Phi_{1,2,3}$ do not mix. As a result there are two existing physical Nambu-Goldstone (NG) bosons originating from the SM-singlet scalars. Because of the tiny quartic couplings and gauge couplings, the SM-singlet scalars become decoupled from the SM thermal bath in the early Universe. Additionally, we consider that the singlet scalars are heavier than the neutral BSM gauge boson Z' preventing its decay into the NG bosons. The breaking of general U(1) gauge symmetry helps Z' to acquire the mass which could be given by

$$
M_{Z'} = g_X \sqrt{64v_1^2 + 100v_2^2 + 9v_3^2 + \frac{1}{4}x_H^2 v_{h_1}^2 + \left(-\frac{1}{2}x_H + 3\right)^2 v_{h_2}^2} \simeq g_X \sqrt{64v_1^2 + 100v_2^2 + 9v_3^2}, \qquad (11)
$$

which is a free parameter and the general $U(1)_X$ gauge coupling g_X is also a free parameter. Because of the general $U(1)_X$ gauge structure, H_2 only couples with $N_R^{1,2}$, making this case a neutrinophilic two Higgs doublet model framework [113,116–119].

C. Z' interactions with the fermions

After the anomaly cancellation conditions are imposed, we notice that Z' in the above models can interact with the left- and right-handed SM fermions differently, manifesting the chiral nature of the models. Fixing $x_\Phi = 1$ in case I, we find that the chiral nature is the same as in case II. Therefore, we write the interactions between the fermions with the Z' in the following as

$$
\mathcal{L}_{\text{int}} = -g_X(\bar{f}\gamma_\mu q_{f_L} P_L f + \bar{f}\gamma_\mu q_{f_R} P_R f) Z'_\mu, \qquad (12)
$$

where $P_{L(R)} = (1 \pm \gamma_5)/2$, and q_{f_L} and q_{f_R} are the corresponding general U(1) charges of the left-handed (f_L) and

TABLE III. Vector and axial vector couplings in general $U(1)_X$ scenarios for the couplings between SM fermions and Z'. In the $B-L$ case considering $x_H = 0$ and $x_\Phi = 1$, the axial vector couplings for the charged fermions vanish.

	Vector coupling (c_V)							Axial-vector coupling (c_A)						
SM fermions	$x_H=-2$	-1	-0.5	0	0.5	1	2	$x_H=-2$	-1	-0.5	0	0.5	1	2
Charged lepton (ℓ^α)	$-\frac{3}{4}x_H-1=\frac{1}{2}$	$-\frac{1}{4}$	$-\frac{5}{8}$	-1	$-\frac{11}{8}$	$-\frac{7}{4}$	$-\frac{5}{2}$	$\frac{1}{4}x_H=-\frac{1}{2}$	$-\frac{1}{4}$	$-\frac{1}{8}$	0	$\frac{1}{8}$	$\frac{1}{4}$	$\frac{1}{2}$
SM-like neutrino (ν_L^α)	$\frac{1}{4}x_H+\frac{1}{2}=0$	$\frac{1}{4}$	$\frac{3}{8}$	$\frac{1}{2}$	$\frac{5}{8}$	$\frac{3}{4}$	1	$\frac{1}{4}x_H+\frac{1}{2}=0$	$\frac{1}{4}$	$\frac{3}{8}$	$\frac{1}{2}$	$\frac{5}{8}$	$\frac{3}{4}$	1
Up-type quarks (q_u^α)	$\frac{5}{12}x_H+\frac{1}{3}=-\frac{1}{2}$	$-\frac{1}{12}$	$\frac{1}{8}$	$\frac{1}{3}$	$\frac{13}{24}$	$\frac{3}{4}$	$\frac{7}{6}$	$-\frac{1}{4}x_H=-\frac{1}{2}$	$-\frac{1}{4}$	$-\frac{1}{8}$	0	$\frac{1}{8}$	$\frac{1}{4}$	$\frac{1}{2}$
Down-type quarks (q_d^α)	$-\frac{1}{12}x_H+\frac{1}{3}=-\frac{1}{2}$	$-\frac{1}{4}$	$-\frac{1}{8}$	$\frac{1}{3}$	$\frac{7}{24}$	$\frac{1}{4}$	$\frac{1}{6}$	$-\frac{1}{4}x_H=-\frac{1}{2}$	$-\frac{1}{4}$	$-\frac{1}{8}$	0	$\frac{1}{8}$	$\frac{1}{4}$	$\frac{1}{2}$

right-handed (f_R) fermions. Hence, we write vector coupling ($c_V = \frac{q_{f_L}+q_{f_R}}{2}$) and axial vector coupling ($c_A = \frac{q_{f_L}-q_{f_R}}{2}$) for the SM fermions following the charge assignments of cases I and II in Table III, fixing $x_\Phi = 1$. Hence, we notice that interactions between SM fermions and Z' are chiral in nature in the general $U(1)_X$ extension of the SM. The partial decay width of Z' into different fermions can be calculated using Eq. (12) and we write down the expression as

$$\Gamma(Z' \to \bar{f}f) = N_C \frac{M_{Z'} g_X^2}{24\pi}\left[(q_{f_L}^2 + q_{f_R}^2)\left(1-\frac{m_f^2}{M_{Z'}^2}\right) + 6 q_{f_L} q_{f_R}\frac{m_f^2}{M_{Z'}^2}\right], \tag{13}$$

where m_f is the mass of different SM fermions and $q_{L,R}$ are the functions of x_H. Here, N_C is the color factor being 1 for the SM leptons and 3 for the SM quarks. The light neutrinos (ν_L) are considered to be massless due to their tiny mass, and putting $q_{f_R} = 0$ in Eq. (13), we obtain the partial decay width of Z' into a pair of one generation light neutrinos as

$$\Gamma(Z' \to \nu\nu) = \frac{M_{Z'} g_X^2}{24\pi} q_{f_L}^2, \tag{14}$$

where q_{f_L} is a function of x_H. The Z' gauge boson can decay into a pair of heavy Majorana neutrinos if Z' is heavier than twice the mass of the heavy neutrinos. The corresponding partial decay width into a single generation of heavy neutrino pairs can be written as

$$\Gamma(Z' \to N_R^\alpha N_R^\alpha) = \frac{m_{Z'} g_X^2}{24\pi} q_{N_R}^2 \left(1-4\frac{m_N^2}{M_{Z'}^2}\right)^{\frac{3}{2}}, \tag{15}$$

with q_{N_R} as the general $U(1)_X$ charge of the heavy neutrinos, which can be found from Tables I and II, respectively, and m_N is the mass of the heavy neutrinos. If we consider that the RHNs are heavier than half of the $M_{Z'}$, then the decay of Z' into a pair of RHNs is kinematically forbidden. We find that the $U(1)_X$ charges of the fermions in case II are same as those in case I with $x_\Phi = 1$. As a result, we can utilize the same bounds for both the cases.

D. Neutrino mass

The Yukawa interactions given in Eqs. (2) and (8) lead us to the generation of the neutrino mass mechanism. The general $U(1)_X$ symmetry breaking generates the Majorana mass term for the three (first two) generations of the RHNs in case I (II), where the BSM scalar $\Phi_{(1)}$ is involved. The Dirac mass term is generated after the electroweak symmetry breaking, where the SM Higgs doublet $H_{1(2)}$ is involved in case I (II). The corresponding Dirac and Majorana mass terms are written in Table IV. Finally, the light neutrino mass is generated by the seesaw mechanism to explain the origin of the tiny neutrino mass term and flavor mixing. Following Table IV, the generic formula for the neutrino mass matrix can be written as

$$m_\nu = \begin{pmatrix} 0 & m_D \\ m_D^T & m_N \end{pmatrix}. \tag{16}$$

Diagonalizing the neutrino mass matrix, we find the light neutrino mass eigenvalues to be $-m_D m_N^{-1} m_D^T$. In case II, $N_R^{1,2}$ will generate the neutrino mass; on the other hand, at the tree level N_R^3 will not participate in the neutrino mass generation and it can be considered as a potential dark matter candidate in some scenarios. The neutrino mass generation mechanism and dark matter physics are not the main motivations of this work, however, we provide a simple outline in this paper for completeness because these general $U(1)_X$ scenarios can generate neutrino mass at the tree level from the so-called seesaw mechanism, which is an important aspect for studying such scenarios.

TABLE IV. Dirac and Majorana masses in the neutrino sector. In case II we use the collider constraints to set $(v_1^2+v_2^2+v_3^2) \gg (v_{h_1}^2+v_{h_2}^2)$ and in this case the first two generations are participating in the neutrino mass generation mechanism.

Models	Majorana mass (m_N)	Dirac mass (m_D)
Case I	$m_{N_R^\alpha} = \frac{Y_N^\alpha}{\sqrt{2}} v_\Phi$	$m_D^{\alpha\beta} = \frac{Y_\nu}{\sqrt{2}} v_1$
Case II	$m_{N_R^{1,2}} = \frac{Y_2^{1,2}}{\sqrt{2}} v_1$	$m_D^{1,2} = \frac{Y_1^{1,2}}{\sqrt{2}} v_{h_2}$

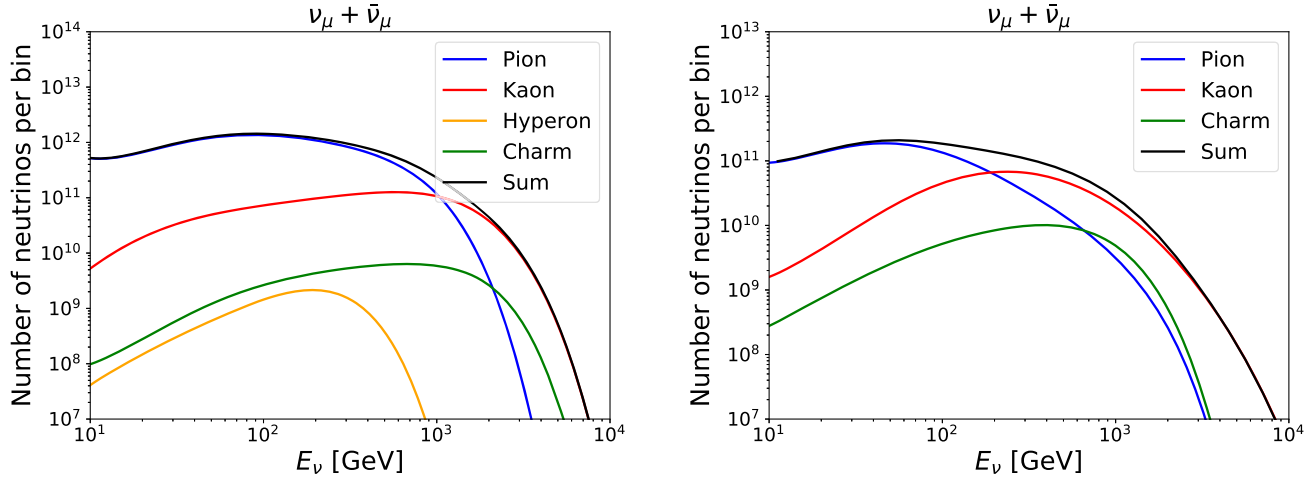

FIG. 1. Number of muon neutrinos pass through the FASERν (left) and SND@LHC (right) detectors. Thirty energy bins are defined uniformly on the logarithmic scale in $[10, 10^4]$ GeV.

III. CALCULATION OF THE CONSTRAINTS ON THE CHIRAL GAUGE COUPLINGS

The chiral Z' gauge boson interacts with the SM fermions, and the couplings depend on the $U(1)_X$ charge of the SM Higgs doublet. Therefore, experiments for scattering measurements of the SM particles can search the chiral Z' gauge boson by measuring deviations of the scattering cross section from the SM value. In this section, we show the scattering cross sections contributed by the chiral Z' gauge boson and methods to calculate constraints on the $U(1)_X$ gauge coupling. In this work, we consider FASER$\nu(2)$, SND@LHC, NA64, and MUonE as the experiments for scattering measurement. In addition, we estimate the constraints from ν-electron, ν-nucleon, electron and proton beam-dump, and long-lived gauge boson searches, respectively.

A. Scattering cross section contributed by chiral Z' at FASER$\nu(2)$, SND@LHC, NA64, and MUonE

In this subsection, we summarize scattering cross sections via chiral Z' interactions at FASER$\nu(2)$, SND@LHC, NA64, and MUonE experiments.

1. Prospects for FASER$\nu(2)$ *and SND@LHC*

The existence of a light Z' affects the neutral-current deep-inelastic scattering at the LHC far-forward detectors. We study the constraints from the FASERν, FASER$\nu2$, and SND@LHC experiments in this subsection. The numbers of neutrinos that pass through the FASERν and SND@LHC detectors have been simulated in Refs. [47,120]. It has been found that the muon neutrino from pion and kaon decay is most abundant, the energy distributions of which are shown in Fig. 1. The corresponding neutrino flux at the FASER$\nu2$ detector can be obtained by rescaling the flux at the FASERν, assuming the neutrino distributes uniformly on the detector surface.

The MG5_aMC@NLO package is used to calculate the fixed target deep-inelastic neutrino-proton scattering cross section at the leading order. Assuming a benchmark detector made of tungsten target, the nCTEQ15FullNuc_184_74 set [121] as implemented in LHAPDF6 [122] is employed as the proton parton distribution function. The partonic collision energy is taken as the factorization and renormalization scales in our simulation. The neutrino-proton scattering cross section $\sigma_{\nu p}$ is related to g_X, x_H, Z' mass as well as the incoming neutrino energy E_ν. In Fig. 2, we present the relation between E_ν and $\sigma_{\nu p}/E_\nu$ for a few sets of x_H and $M_{Z'}$. The g_X is fixed to unity, since the change of g_X can only lead to a total rescaling. The Z' contribution is slightly increased with increasing x_H from -1 to 1. The dependence on the $M_{Z'}$ is more complicated due to the interference effects between the Z and Z' bosons. The Z' contribution is negligible for $M_{Z'} \gtrsim 100$ GeV, and the cross section becomes identical to the SM one in this region. Given the neutrino-nucleus cross section ($\sigma_{\nu N}$, which is $184 \times \sigma_{\nu p}$, the mass number of Tungsten is approximately 184), one can estimate the probability of a neutrino interacting with the detector as

$$P = \frac{\sigma_{\nu N} \times \text{Number of Nuclei}}{\text{Detector Area}} = \frac{\sigma_{\nu N}}{A}\frac{m_{\text{det}}}{m_N}, \quad (17)$$

where N is the target nucleus, A is the detector area, and m_N is the mass of the target nucleus. The relevant detector configurations are listed in Table V.

For given g_X, x_H, and $M_{Z'}$, the number of interacting neutrinos in each E_ν bin can be calculated by the products of the number of neutrinos passing through the detector and the interaction probability. For illustration, energy spectra for the interacting muon neutrino at the FASERν, FASER$\nu2$, and SND@LHC detectors are shown in Fig. 3. The g_X is taken to be the unity. Three different values of x_H and six different values of $M_{Z'}$ are used. The number of

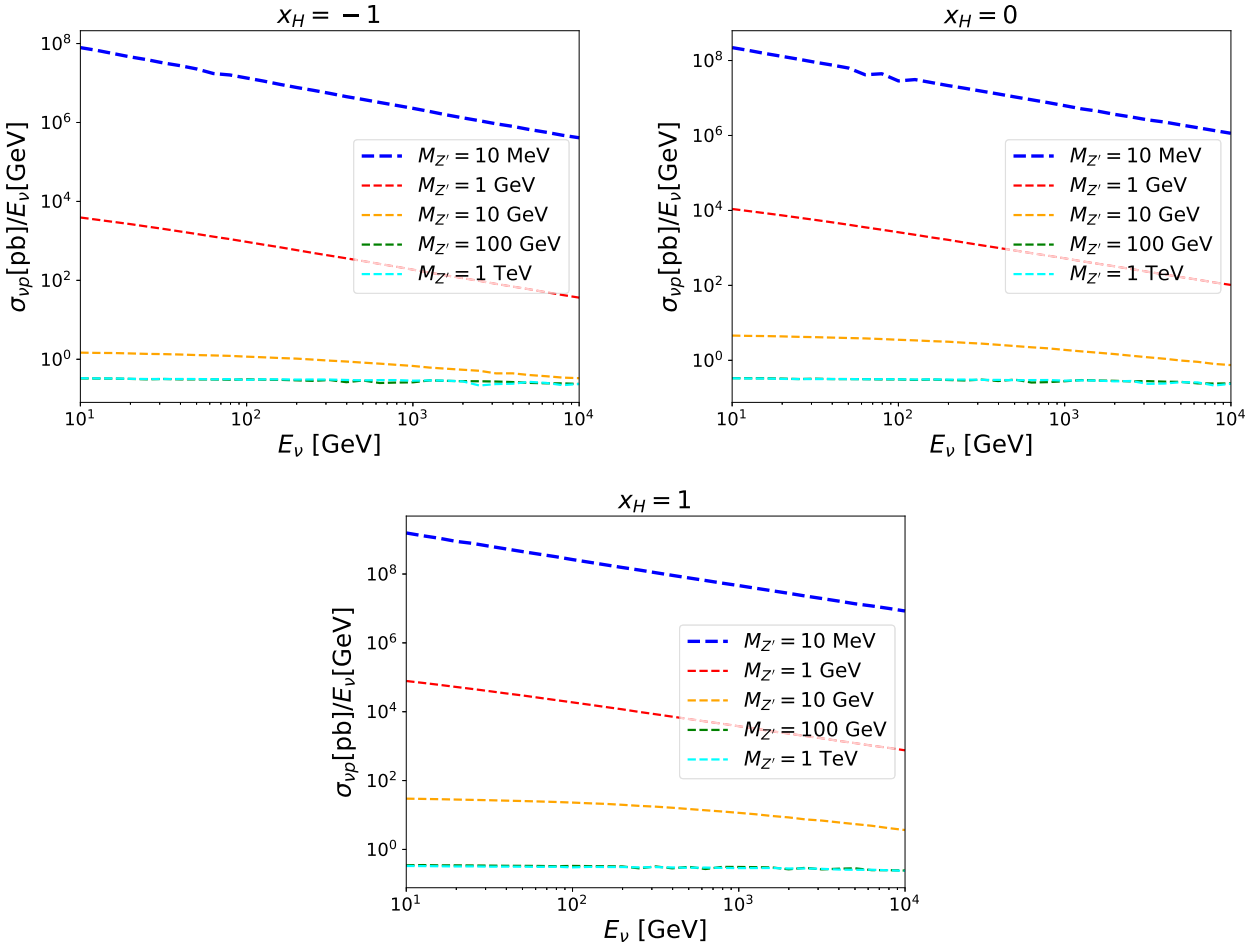

FIG. 2. The neutrino-proton scattering cross section $\sigma_{\nu p}$ divided by the incoming neutrino energy E_ν. The gauge coupling g_X is set to unity.

interacting neutrinos is increased with increasing x_H and decreasing $M_{Z'}$. Moreover, we can observe that the number at the FASERν detector is around 1 order of magnitude larger than that at the SND@LHC detector, while it is around 2 orders of magnitude below that at the FASERν2 detector.

We follow a similar strategy as proposed in Ref. [33] to estimate the sensitivity reach in the parameter space of g_X and $M_{Z'}$ for our model. Only the total numbers of interacting neutrinos are used in defining the χ^2 measure (i.e., the shape of E_ν spectra are not of concern),

$$\chi^2 = \min_\alpha \left[\frac{N^{\nu_e}_{\rm BSM} - (1+\alpha)N^{\nu_e}_{\rm SM}}{N^{\nu_e}_{\rm BSM}} + \frac{N^{\nu_\mu}_{\rm BSM} - (1+\alpha)N^{\nu_\mu}_{\rm SM}}{N^{\nu_\mu}_{\rm BSM}} + \frac{N^{\nu_\tau}_{\rm BSM} - (1+\alpha)N^{\nu_\tau}_{\rm SM}}{N^{\nu_\tau}_{\rm BSM}} + \left(\frac{\alpha}{\sigma_{\rm norm}}\right)^2 \right], \tag{18}$$

where $N_{\rm BSM}$ and $N_{\rm SM}$ are the number of interacting neutrinos of each flavor in our model and in the SM model. The systematic uncertainties ($\sigma_{\rm norm}$) in each neutrino flavor are assumed to be the same and only one nuisance parameter α is used. The χ^2 value is obtained by minimizing over the α. The 95% confidence level sensitivity reach corresponds to $\chi^2 = 3.84$.

TABLE V. Detector configurations.

Detector	A (cm)	$m_{\rm det}$ (ton)	Integrated luminosity (fb^{-1})
FASERν	25×25	1.2	150
FASERν2	50×50	10	3000
SND@LHC	39×39	0.8	150

2. Constraints from the NA64

The fixed-target experiment NA64 at the CERN Super Proton Synchrotron [57,58] aims to search for the Z' that is produced through the bremsstrahlung process in the high-energy electron beam colliding with heavy nuclei,

$$e^- Z \to e^- Z Z'; \quad Z' \to \nu\nu, \tag{19}$$

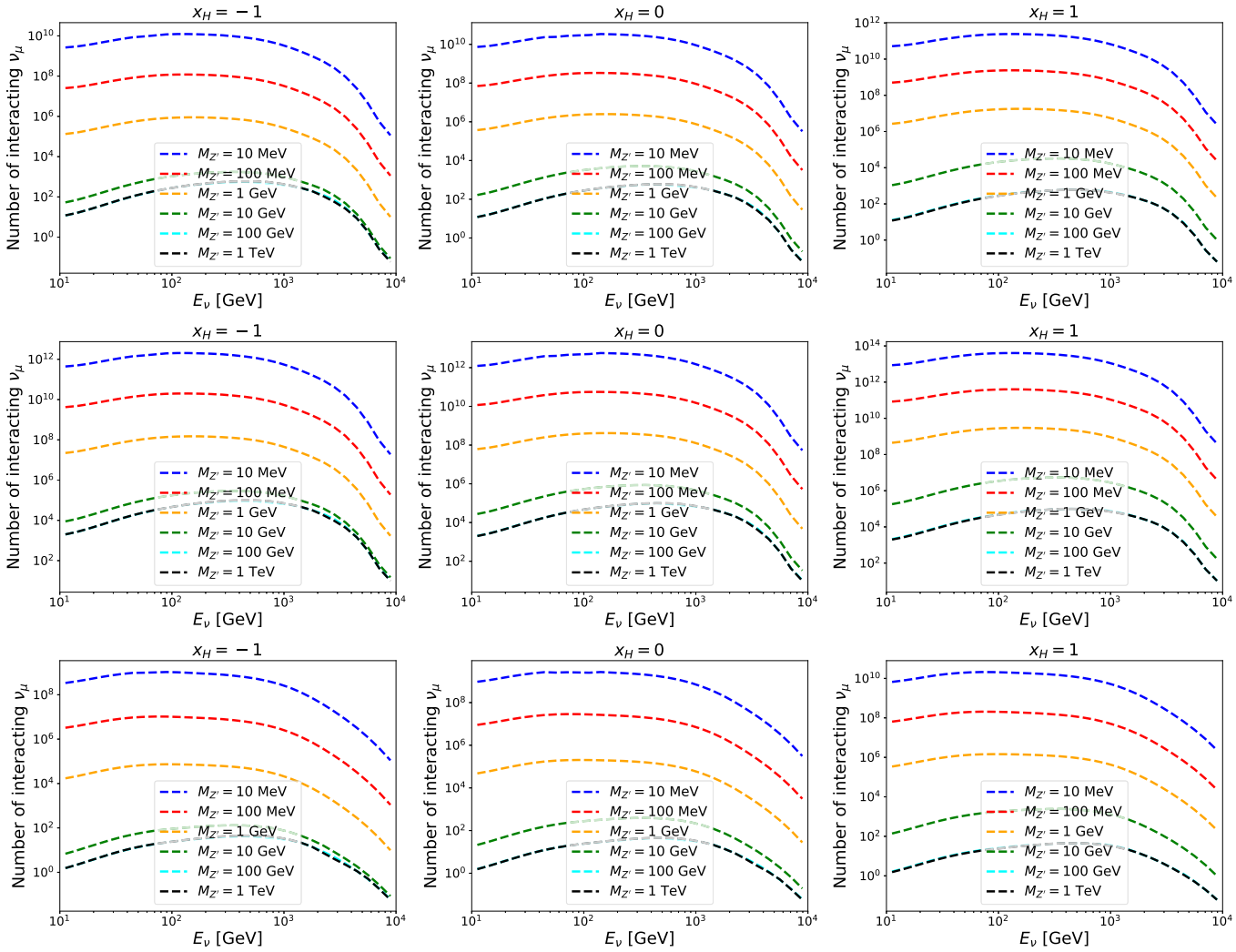

FIG. 3. The muon neutrino spectra at the FASERν (top), FASERν2 (middle) and SND@LHC (bottom) detectors.

where the Z' is decaying invisibly. The partial width of each Z' decay channel is calculated by the DarkCast package [12,14], assuming that only vector interactions exist. The results are translated into those in our chiral model by using the same method as we proposed in Ref. [10].

The production cross section and the energy spectrum of the Z' is simulated by the MG5_aMC@NLO package. Since the target nucleus is led at the NA64 experiment, the nCTEQ15_208_82 set in LHAPDF6 is employed as the proton PDF. The total cross section is proportional to g_X^2. Taking $g_X = 0.2$ and incoming electron beam energy $E_0 = 100$ GeV, we present the electron-proton scattering cross sections with respect to varying x_H and $M_{Z'}$ in the left panel of Fig. 4. It can be observed that the cross section is increased with increasing x_H and decreasing $M_{Z'}$. In the right panel of Fig. 4, the normalized bremsstrahlung Z' spectra are shown. The shape of the Z' spectrum is highly dependent on the Z' mass, while it is almost irrelevant to the x_H value. Some analytic discussions about the feature of the spectrum are conducted in Ref. [123].

Having calculated the differential bremsstrahlung Z' production cross section ($d\sigma_{Z'}/dE_{Z'}$) as well as the Z' decay branching ratios for all of the channels, we are able to calculate the number of signal events at the NA64 experiment as follows [56]:

$$n_{Z'}(g_X, x_H, M_{Z'}) = \int_{0.5E_e}^{E_e} C \frac{d\sigma_{Z'}}{dE_{Z'}} \left[\mathrm{Br}(Z' \to \nu\nu) + \sum_l \mathrm{Br}(Z' \to l^+ l^-) \right] \times \exp\left(-\frac{L_{\mathrm{ECAL}} + L_{\mathrm{HCAL}}}{L_{Z'}} \right) \Bigg], \tag{20}$$

where C is related to the detector parameters. The $L_{Z'} = c\tau_{Z'} E_{Z'}/M_{Z'}$, L_{ECAL}, and L_{HCAL} are the Z' decay length, electromagnetic calorimeter length, and hadronic calorimeter length, respectively. Reference [56] uses data with 3.22×10^{11} electrons on target collected during 2016–2021 runs at the NA64 experiment and obtains the 90% C.L. exclusion limits for the $U(1)_{B-L}$ model. The corresponding

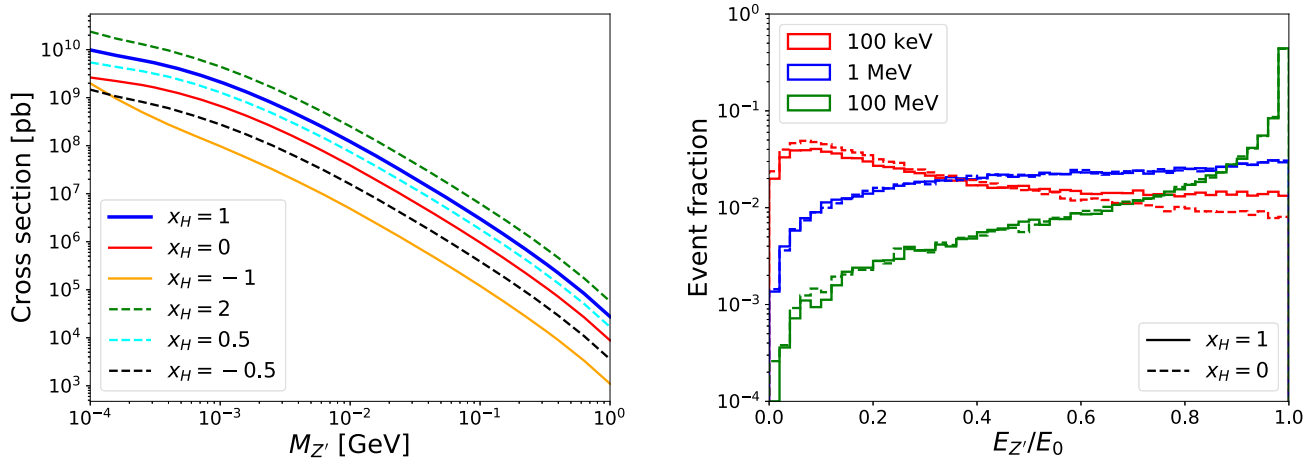

FIG. 4. Left: the total cross section for the bremsstrahlung Z' production. Right: normalized $E_{Z'}/E_0$ distribution for different Z' masses. $E_0 = 100$ GeV is the electron beam energy.

bounds for our chiral model with different x_H can be obtained by requiring the number of signal events $n_{Z'}(g_X, x_H, M_{Z'})$ in Eq. (20) to be the same as that in the $B-L$ case.

3. Constraints from the MUonE

MUonE [124,125] is an experiment at CERN aiming to measure elastic scatterings between the 150 GeV μ^+ beam and target being electrons in beryllium atoms and determining a contribution of hadronic vacuum polarization to the muon anomalous magnetic moment with a method [126]. The existence of the chiral Z' changes the cross section of the elastic scattering between the positive muon and electron, and therefore, the chiral Z' can be searched by estimating a deviation of the scattering cross section from the SM prediction.

The elastic scattering cross section between the positive muon and electron is given by

$$\frac{d\sigma(\mu^+e^-)}{dT} = \left.\frac{d\sigma(\mu^+e^-)}{dT}\right|_{\rm SM} + \left.\frac{d\sigma(\mu^+e^-)}{dT}\right|_{Z'} + \left.\frac{d\sigma(\mu^+e^-)}{dT}\right|_{\rm Int}, \tag{21}$$

where T denotes the electron recoil energy, and the first, second, and third terms on the right-hand side (rhs) correspond to the contributions from only the SM interaction, only the Z' one, and the interference between the SM and Z' ones. The purely SM contribution can be given by

$$\left.\frac{d\sigma(\mu^+e^-)}{dT}\right|_{\rm SM} = \frac{\pi\alpha_{\rm EM}^2}{(E_\mu^2 - m_\mu^2)m_e^2(T-m_e)^2}\{2E_\mu m_e(E_\mu - T + m_e) - (T-m_e)(2m_e^2 + m_\mu^2 - m_e T)\}, \tag{22}$$

where $\alpha_{\rm EM}$ denotes the fine-structure constant, and E_μ stands for the energy of the positive muon. The contributions from Z' exchanging diagram and interference between the SM and Z' are estimated by

$$\begin{aligned}\left.\frac{d\sigma(\mu^+e^-)}{dT}\right|_{Z'} = {}& \frac{g_X^4 m_e}{128\pi M_{Z'}^4(E_\mu^2 - m_\mu^2)(M_{Z'}^2 + 2m_e T - m_e^2)^2} \\ & \times [(\tilde{x}_e + \tilde{x}_\ell)^4\{M_{Z'}^4(2E_\mu(E_\mu - T + m_e) + T^2 - 3m_e T - m_\mu^2 + 2m_e^2)\} \\ & + 2(\tilde{x}_e + \tilde{x}_\ell)^3(\tilde{x}_e - \tilde{x}_\ell)\{M_{Z'}^4(2E_\mu^2 - m_e T - m_\mu^2 + m_e^2)\} + 2(\tilde{x}_e + \tilde{x}_\ell)^2(\tilde{x}_e - \tilde{x}_\ell)^2 \\ & \times \{M_{Z'}^4(2E_\mu(E_\mu + T - m_e) - (T-m_e)^2) + 2m_e m_\mu^2 M_{Z'}^2(T-m_e) + 2m_e^2 m_\mu^2(T-m_e)^2\} \\ & + 2(\tilde{x}_e + \tilde{x}_\ell)(\tilde{x}_e - \tilde{x}_\ell)^3\{M_{Z'}^4(2E_\mu^2 + m_e T + m_\mu^2 - m_e^2) + 4m_e m_\mu^2 M_{Z'}^2(T-m_e) + 4m_e^2 m_\mu^2(T-m_e)^2\} \\ & + (\tilde{x}_e - \tilde{x}_\ell)^4\{M_{Z'}^4(2E_\mu(E_\mu - T + m_e) + T^2 - m_e T + m_\mu^2) + 4m_e m_\mu^2 M_{Z'}^2(T-m_e) + 4m_e^2 m_\mu^2(T-m_e)^2\}], \end{aligned} \tag{23}$$

$$\begin{aligned}\left.\frac{d\sigma(\mu^+e^-)}{dT}\right|_{\rm Int} = {}& \frac{\alpha_{\rm EM} g_X^2}{8(E_\mu^2 - m_\mu^2)(T-m_e)(M_{Z'}^2 + 2m_e T - m_e^2)}[(\tilde{x}_e + \tilde{x}_\ell)^2\{2E_\mu(E_\mu - T + m_e) + T^2 - 3m_e T - m_\mu^2 + 2m_e^2\} \\ & + (\tilde{x}_e + \tilde{x}_\ell)(\tilde{x}_e - \tilde{x}_\ell)(2E_\mu^2 - m_e T - m_\mu^2 + m_e^2) + (\tilde{x}_e - \tilde{x}_\ell)^2(T-m_e)(2E_\mu - T + m_e)]. \end{aligned} \tag{24}$$

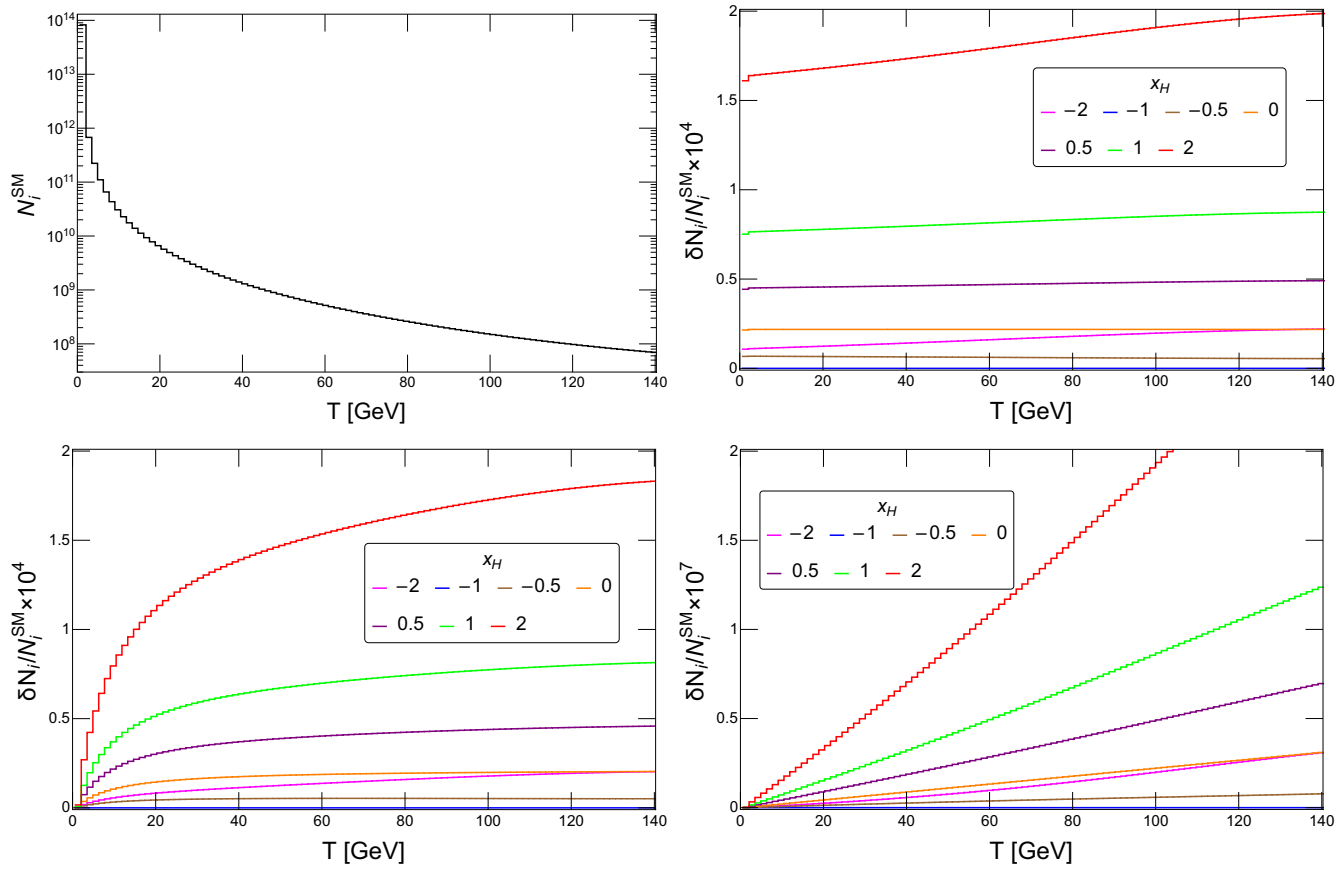

FIG. 5. Top-left: the distribution of the number of events contributed only by the SM particles in MUonE. Top-right, bottom-left, and bottom-right panels: the distributions of the deviation of the number of events in MUonE from that contributed only by the SM particles: $\delta N_i/N_i^{\rm SM} \equiv (N_i^{\rm SM+Z'} - N_i^{\rm SM})/N_i^{\rm SM}$ for $(M_{Z'}/{\rm GeV}, g_X) = (10^{-3}, 10^{-3}), (10^{-1}, 10^{-3}), (10, 10^{-3})$, respectively.

The number of elastic scattering signals in the ith bin of the electron recoil energy ($T_i < T < T_i + \Delta T$) is evaluated by [35]

$$N_i = \mathcal{L} \int_{T_i}^{T_i+\Delta T} dT \frac{d\sigma(\mu^+ e^-)}{dT} \Theta(T)\Theta(T_{\rm max}(E_\mu) - T), \tag{25}$$

where $\mathcal{L}$ is the integrated luminosity, and $\mathcal{L} = 150$ fb^{-1} for MUonE. In Eq. (25), $\Theta(T)$ is the Heaviside step function, and $T_{\rm max}(E_\mu)$ stands for the maximal value of the electron recoil energy determined by

$$T_{\rm max}(E_\mu) = \frac{2m_e(E_\mu^2 - m_\mu^2)}{2E_\mu m_e + m_e^2 + m_\mu^2}. \tag{26}$$

In Fig. 5, the number of events contributed only by the SM particles and the deviation of the number of events in the chiral Z' model from that in the SM are shown.

In this paper, we evaluate the sensitivity of MUonE to the chiral Z' gauge boson by the χ^2 function, following Ref. [35]. The χ^2 function is calculated by

$$\chi^2 = \sum_{i=1}^{100} \frac{(N_i - N_i^{\rm SM})^2}{\sigma_{{\rm stat},i}^2 + \sigma_{{\rm sys},i}^2}, \tag{27}$$

where $\sigma_{{\rm stat},i} = \sqrt{N_i}$ stands for the statistical uncertainty, and $\sigma_{{\rm sys},i} = 10^{-5} N_i$ stands for the systematic uncertainty at the level of 10 ppm [124]. The 95% confidence level sensitivity is obtained by solving $\chi^2 = 3.84$.

B. Constraints from proton/electron beam-dump experiments

For constraints from proton beam-dump experiments NOMAD and CHARM, we obtain bound curves by rescaling the bounds of the $U(1)_{B-L}$ case given in Ref. [11]. The upper bound on the $\{m_{Z'}, g_X\}$ plane is approximately derived applying scaling [12,29]

$$\tau_{Z'}(g_{B-L}^{\rm max}) \sim \tau_{Z'}(g_X^{\rm max}, x_H, x_\Phi), \tag{28}$$

where g_{B-L} denotes the gauge coupling in the $U(1)_{B-L}$ case, and $\tau_{Z'}$ is the lifetime of the Z'. The lower bound is also scaled by applying

$$g_X^{\rm low} \sim g_{B-L}^{\rm low}\sqrt{\frac{{\rm Br}(M\to Z'_{B-L}\gamma){\rm Br}(Z'_{B-L}\to e^+e^-)\tilde{\tau}_{Z'}}{{\rm Br}(M\to Z'\gamma){\rm Br}(Z'\to e^+e^-)\tilde{\tau}_{Z'_{B-L}}}}, \tag{29}$$

where $\tilde{\tau}$ is lifetime with gauge coupling being unity, and Z' is produced via meson decay with $M=\pi^0$ for MONAD and $M=\eta$ for CHARM dominantly. The ratio of meson decay branching ratio thus represents the ratio of Z' production cross sections. Here, the meson decay branching ratio is estimated using the method given in Ref. [12]. In addition to that, we use the same rescaling technique to estimate the constraints on the $\{M_{Z'}, g_X\}$ plane from the FASER [127] and NA62 [128] experiments for different $U(1)_X$ charges, where the ratio of Z' production cross section between dark photon and $U(1)_X$ cases is estimated by calculating the bremsstrahlung process as a good approximation using the method in Ref. [10].

For the proton beam-dump experiment ν-cal, the bremsstrahlung process dominantly produces the Z' boson. In this work, we use the excluded region given in Ref. [10] on $\{M_{Z'}, g_X\}$ space, where we take into account chiral structure of the Z' interactions in estimating the Z' production cross section.

For electron beam-dump constraints from Orsay and KEK, The bound curves are obtained by rescaling the bounds of the $U(1)_{B-L}$ case as for the proton beam-dump one. We derive the constraint on the upper region on the $\{M_{Z'}, g_X\}$ plane approximately by scaling with Eq. (28), which is the same as the proton beam-dump case. On the other hand, the constraint on the lower region is estimated by [29]

$$g_X^{\rm low} \sim g_{B-L}^{\rm low} \times\sqrt{\frac{2{\rm Br}(Z'_{B-L}\to e^+e^-)\tilde{\tau}_{Z'}}{(5x_H^2/4+3x_Hx_\Phi+2x_\Phi^2){\rm Br}(Z'\to e^+e^-)\tilde{\tau}_{Z'_{B-L}}}}, \tag{30}$$

where Z' is considered to be produced via bremsstrahlung process.

For electron beam-dump constraints from E137 and E141 experiments, we use the results in Ref. [10] for the excluded region on $\{M_{Z'}, g_X\}$ in which the chiral structure of the Z' interactions is taken into account in estimating the Z' production cross section via bremsstrahlung process.

C. Constraints from electron-(anti)neutrino scattering in neutrino experiments

Here we discuss constraints on $\{M_{Z'}, g_X\}$ from electron-(anti)neutrino scattering processes that are tested by neutrino experiments: BOREXINO, TEXONO, GEMMA, CHARM-II, and the J-PARC Sterile Neutrino Search at the J-PARC Spallation Neutron Source (JSNS2). To obtain the constraints, we estimate the electron-(anti)neutrino scattering cross sections under the existence of Z' interactions. The differential cross section can be expressed as

$$\frac{d\sigma(\nu e)}{dT} = \left.\frac{d\sigma(\nu e)}{dT}\right|_{\rm SM} + \left.\frac{d\sigma(\nu e)}{dT}\right|_{Z'} + \left.\frac{d\sigma(\nu e)}{dT}\right|_{\rm Int}, \tag{31}$$

where T denotes the electron recoil energy and the first, second, and third terms on the rhs correspond to the contributions from the only SM interactions, the only Z' interactions, and interference between the SM and Z' interactions. The terms on the rhs are given as follows [29]. The purely SM contribution can be written by

$$\left.\frac{d\sigma(\nu e)}{dT}\right|_{\rm SM} = \frac{2G_F^2 m_e}{\pi E_\nu^2}(a_1^2E_\nu^2 + a_2^2(E_\nu - T)^2 - a_1a_2m_eT), \tag{32}$$

where E_ν is the energy of the initial neutrino. Here a_1 and a_2 are given by

$$a_1 = \left\{\sin^2\theta_W + \frac{1}{2}, \sin^2\theta_W, \sin^2\theta_W - \frac{1}{2}, \sin^2\theta_W\right\} \quad \text{for } \{\nu_e e, \bar{\nu}_e e, \nu_\beta e, \bar{\nu}_\beta e\}, \tag{33}$$

$$a_2 = \left\{\sin^2\theta_W, \sin^2\theta_W + \frac{1}{2}, \sin^2\theta_W, \sin^2\theta_W - \frac{1}{2}\right\} \quad \text{for } \{\nu_e e, \bar{\nu}_e e, \nu_\beta e, \bar{\nu}_\beta e\}, \tag{34}$$

where $\beta = \{\mu, \tau\}$. The contribution from the Z' exchanging diagram is estimated by

$$\left.\frac{d\sigma(\overset{(-)}{\nu}{}_\alpha e)}{dT}\right|_{Z'} = \frac{g_X^4(\tilde{x}_\ell)^2 m_e}{4\pi E_\nu^2(2m_eT + M_{Z'}^2)}[(2E_\nu^2 - 2E_\nu T + T^2)(b_1^2 + b_2^2) \pm 2b_1b_2(2E_\nu - T)T - m_eT(b_1^2 - b_2^2)], \tag{35}$$

where $b_1 = \frac{\tilde{x}_\ell + \tilde{x}_e}{2}$ and $b_2 = \frac{\tilde{x}_\ell - \tilde{x}_e}{2}$ with $\tilde{x}_{\ell,e}$ from Table I, and the negative sign of $\pm$ is for the process of the antineutrino. The contributions from interference between the SM and Z' are also written, depending on the process, as follows:

$$\left.\frac{d\sigma(\nu_e e)}{dT}\right|_{\rm int} = \frac{G_F g_X^2 \tilde{x}_\ell m_e}{\sqrt{2}\pi E_\nu^2 (2m_e T + M_{Z'}^2)} [2E_\nu^2(b_1+b_2) + (2E_\nu^2 - 2E_\nu T + T^2)(b_1 c_1 + b_2 c_2)] + T(2E_\nu - T)(b_1 c_2 + b_2 c_1) - m_e T(b_1 - b_2 + b_1 c_1 - b_2 c_2)], \tag{36}$$

$$\left.\frac{d\sigma(\bar{\nu}_e e)}{dT}\right|_{\rm int} = \frac{G_F g_X^2 \tilde{x}_\ell m_e}{\sqrt{2}\pi E_\nu^2 (2m_e T + M_{Z'}^2)} [2(E_\nu - T)^2(b_1+b_2) + (2E_\nu^2 - 2E_\nu T + T^2)(b_1 c_1 + b_2 c_2)] - T(2E_\nu - T)(b_1 c_2 + b_2 c_1) - m_e T(b_1 - b_2 + b_1 c_1 - b_2 c_2)], \tag{37}$$

$$\left.\frac{d\sigma((\overset{\nu}{-})_\beta e)}{dT}\right|_{\rm int} = \frac{G_F g_X^2 \tilde{x}_\ell m_e}{\sqrt{2}\pi E_\nu^2 (2m_e T + M_{Z'}^2)} [(2E_\nu^2 - 2E_\nu T - T^2)2(b_1 c_1 + b_2 c_1) \pm T(2E_\nu - T)(b_1 c_2 + b_2 c_1)] - m_e T(b_1 c_1 - b_2 c_2)], \tag{38}$$

where $c_1 = -1/2 + 2\sin^2\theta_W$ and $c_2 = -1/2$. We then estimate the differential cross sections and derive the constraints for each experiment in the following way.

BOREXINO: The cross section of the $\nu_e - e$ scattering process is estimated by the experiment, where $\langle E_\nu \rangle = 862$ keV and $T \simeq [270, 665]$ keV for the ^7B_e solar neutrino. We require that the cross section with Z' interaction should not be more than 8% above that of the SM prediction [74] to obtain the constraint on $\{M_{Z'}, g_X\}$.

TEXONO: $\bar{\nu}_e$-e scattering process is measured by the experiment using 187 kg of CsI(Tl) scintillating crystal array with 29882/7369 kg-day of reactor ON/OFF data with electron recoil energy of $T \simeq [3, 8]$ MeV. The χ^2 value is estimated as

$$\chi^2 = \sum_{\rm bin} \frac{(R_{\rm data} - R_{\rm th})^2}{\Delta R^2}, \tag{39}$$

where $R_{\rm data}$ and $R_{\rm th}$ are the event ratios measured by the experiment and predicted by the cross section in Eq. (31), and ΔR is the experimental uncertainty, for each recoil energy bin taken from data in Ref. [70]. Here we also applied antineutrino flux in the reference. The constraint on the $\{M_{Z'}, g_X\}$ plane is then obtained by χ^2 analysis with 90% C.L.

GEMMA: $\bar{\nu}_e$-e scattering is observed with 1.5 kg high-purity germanium detector where energy of the neutrino is $\langle E_\nu \rangle \sim 1$–$2$ MeV and flux is 2.7×10^{13} cm^{-2} s^{-1}. The χ^2 value is estimated applying the formula (39) for the data given in Ref. [129] with 13000 on hours and 3000 off hours, and we derive the upper limit curve on $\{M_{Z'}, g_X\}$ with 90% C.L.

CHARM-II: $\nu_\mu(\bar{\nu}_\mu)$-electron scattering is observed where 2677 ± 82 and 2752 ± 88 events are, respectively, obtained for ν_μ and $\bar{\nu}_\mu$ cases. The mean neutrino energies for ν_μ and $\bar{\nu}_\mu$ are, respectively, $\langle E_{\nu_\mu} \rangle = 23.7$ and $\langle E_{\bar{\nu}_\mu} \rangle = 19.1$ GeV, and the range of the observed recoil energy is 3–24 GeV. The χ^2 value is estimated using the formula (39) for the data given in Refs. [82,83], and we derive the upper curve on $\{M_{Z'}, g_X\}$ with 90% C.L.

JSNS2: In the experiment, a 3 GeV proton collides with the mercury target producing pions giving neutrino beams. We consider $\nu_e - e$ and $\bar{\nu}_\mu - e$ scattering processes to obtain the constraint. We estimate the number of scattering events applying 3.8×10^{22} protons on target per year, 17 tons of a gadolinium-loaded liquid-scintillator detector, and neutrino fluxes given in Ref. [79]. The corresponding χ^2 is estimated by

$$\chi^2 = \min_\alpha \left[\frac{(N_{\rm th} - (1+\alpha)N_{\rm SM})^2}{N_{\rm th}} + \left(\frac{\alpha}{\sigma_{\rm norm}}\right)^2 \right], \tag{40}$$

where $N_{\rm th}$ and $N_{\rm SM}$ are the expected number of events in our models and in the SM for 1 yr, $\sigma_{\rm norm}$ is the systematic uncertainty in the neutrino flux normalization, and α is a nuisance parameter. Here $\sigma_{\rm norm}$ is assumed to be 5% as the reference value. Then the future sensitivity on the $\{M_{Z'}, g_X\}$ plane is estimated by requiring the χ^2 value to be less than that of 90% C.L.

D. Limits from coherent neutrino-nucleus scattering

An upper limit curve on $\{M_{Z'}, g_X\}$ is also obtained from coherent elastic neutrino-nucleus scattering (CEνNS) that is measured by the COHERENT experiment with CsI and Ar targets [87,130,131]. Here we derive the curve by rescaling the limit curve for the $U(1)_{B-L}$ case given in Refs. [43,86] by comparing the number of events in $U(1)_{B-L}$ and other cases. We estimate the number of events at the COHERENT experiment adopting formulas in the reference, as discussed below.

First, the differential cross section for the CEνNS process is estimated by [132,133]

$$\frac{d\sigma_{\nu-N}}{dT}(E,T) = \frac{G_F^2 M}{\pi}\left(1 - \frac{MT}{2E^2}\right) Q^2_{\rm SM+Z'}, \tag{41}$$

where E is the initial neutrino energy, T is the recoil energy, M is the mass of the target nucleus, and $Q_{\mathrm{SM}+Z'}$ is the factor coming from interactions including SM and Z' gauge bosons. In our models, $Q_{\mathrm{SM}+Z'}$ is given by

$$Q_{\mathrm{SM}+Z'} = (g_V^p(\nu_\ell) + 2\epsilon_{\ell\ell}^{uV} + \epsilon_{\ell\ell}^{dV})ZF_Z(|\mathbf{q}^2|) + (g_V^n(\nu_\ell) + \epsilon_{\ell\ell}^{uV} + 2\epsilon_{\ell\ell}^{dV})NF_N(|\mathbf{q}^2|), \quad (42)$$

where $g_V^{p(n)}$ is the neutrino-proton (neutron) coupling in the SM, Z (N) is the number of protons (neutrons) in the target nucleus, and $F_{Z(N)}(|\mathbf{q}^2|)$ are the form factors of the proton (neutron) for the target nucleus. The $\epsilon_{\ell\ell}^{qV}$ is the effective coupling explicitly given by

$$\epsilon_{\ell\ell}^{qV} = \frac{g_X^2 \tilde{x}_\ell \tilde{x}_q}{\sqrt{2}G_F(\mathbf{q}^2 + M_{Z'}^2)}. \quad (43)$$

We adopt the values of $g_V^p(\nu_e) = 0.0401$, $g_V^p = 0.0318$, and $g_V^n = -0.5094$ for the neutrino-proton (neutron) coupling in the SM [134,135]. The Helm parametrization [136] is applied for the form factors $F_{Z(N)}(|\mathbf{q}^2|)$ using proton rms radii $\{R_p(\mathrm{Cs}), R_p(\mathrm{I}), R_p(\mathrm{Ar})\} = \{4.804, 4.749, 3.448\}$ (fm) and neutron rms radii $\{R_n(\mathrm{Cs}), R_n(\mathrm{I}), R_n(\mathrm{Ar})\} = \{5.01, 4.94, 3.55\}$ (fm) [137–139].

Then we adopt the neutrino fluxes for the CEνNS event rate in the experiment which depend on the neutrino fluxes produced from the Spallation Neutron Source at the Oak Ridge National Laboratory. They are given by [87,131]

$$\frac{dN_{\nu_\mu}}{dE} = \eta\delta\left(E - \frac{m_\pi^2 - m_\mu^2}{2m_\pi}\right), \quad (44)$$

$$\frac{dN_{\nu_{\bar{\mu}}}}{dE} = \eta\frac{64E^2}{m_\mu^3}\left(\frac{3}{4} - \frac{E}{m_\mu}\right), \quad (45)$$

$$\frac{dN_{\nu_e}}{dE} = \eta\frac{192E^2}{m_\mu^3}\left(\frac{1}{2} - \frac{E}{m_\mu}\right), \quad (46)$$

where $\eta = rN_{\mathrm{POT}}/(4\pi L^2)$ with L, N_{POT}, and r being, respectively, the distance between the source and the detector, the number of protons-on-target (POT), and the number of neutrinos per flavor that are produced for each POT. For these values, we use $r = 9 \times 10^{-2}$, $N_{\mathrm{POT}} = 13.7 \times 10^{22}$, and $L = 27.5$ m for the Ar detector and $r = 0.08$, $N_{\mathrm{POT}} = 17.6 \times 10^{22}$, and $L = 19.5$ m for the CsI detector, respectively.

Finally, the theoretical number of events for each energy bin in the experiment is derived from

$$N_i = N(\mathcal{N})\int_{T_i}^{T_{i+1}} dT A(T)\int_{E_{\min}}^{E_{\max}} dE \sum_{\nu=\nu_e,\nu_\mu,\nu_{\bar{\mu}}} \frac{dN_\nu}{dE}\frac{d\sigma_{\nu-N}}{dT} \times (E,T), \quad (47)$$

where i corresponds to each recoil energy bin, $E_{\min(\max)} = \sqrt{MT/2}(m_\mu/2)$, and $A(T)$ is the energy-dependent reconstruction efficiency. We estimate the upper limit of the coupling g_X for each Z' mass for different models by rescaling that of the $U(1)_{B-L}$ case in Ref. [86] by comparing the number of events for the upper limit of g_X in $U(1)_{B-L}$ with the number of events in each model.

E. Limits from collider experiments: LEP-II, CMS, LHCb, and *BABAR*

Here we briefly summarize our estimation of limit on $\{M_{Z'}, g_X\}$ from results of several collider experiments:

(i) The limit from LEP-II: We estimate the upper limit curve on $\{M_{Z'}, g_X\}$ from the results of LEP-II [100,140] that measure $e^+e^- \to \bar{f}f$ scattering cross sections at the Z peak with f being the SM fermions. The scattering cross sections are estimated including the Z' exchanging diagram in addition to the SM processes. Then the value of the cross section is compared with the observed value. As a result, we consider constraints coming from the cross section of the $e^+e^- \to q\bar{q}$ process, giving the hadronic final state whose value is $\sigma = 41.544 \pm 0.037$ nb, and the $e^+e^- \to \ell^+\ell^-$ process with $R_\ell = \Gamma_{had}/\Gamma_\ell = 20.768 \pm 0.024$. We thus obtain the upper limit of g_X as a function of $m_{Z'}$ when we require the total cross section to be within the 90% C.L. of the observed value.

(ii) The limit from dark photon search at the LHC experiments: The bounds on $\{M_{Z'}, g_X\}$ are also obtained from the results of CMS [90] and LHCb [141] experiments searching for dark photon A' which decays into the $\mu^+\mu^-$ pair. They provide us the bounds on the mass of dark photon $m_{A'}$ and kinetic mixing parameter ϵ. The upper limit on g_X as a function of $M_{Z'}$ can be estimated using the following rescaling:

$$g_X^{\max}(M_{Z'} = m_{A'}) = \epsilon^{\max}(m_{A'})e\sqrt{\frac{\sigma(pp \to A')\mathrm{Br}(A' \to \mu^+\mu^-)}{\sigma(pp \to Z')\mathrm{Br}(Z' \to \mu^+\mu^-)}}, \quad (48)$$

where $\sigma(pp \to A'(Z'))$ is the dark photon (Z') production cross section estimated by CalcHEP3.5 [142] implementing relevant interactions, and $\epsilon^{\max}(m_{A'})$ is the upper limit of the kinetic mixing parameter as a function of dark photon mass.

(iii) The limit from the *BABAR* experiment: At the *BABAR* experiment, the dark photon is searched for via the process $e^+e^- \to A'\gamma$ [91,92]. They consider visible A' which decays into $\{e^+e^-, \mu^+\mu^-$, light mesons$\}$ final states and invisible A' which decays into an invisible final state such as neutrinos. To estimate the bounds on g_X, we rescale the upper limit of gauge coupling in the $U(1)_{B-L}$ case given in Ref. [11] as a function of Z' mass. The rescaling formula for the visible Z' decay mode is

$$g_X^{\max}(M_{Z'}) = g_{B-L}^{\max}(M_{Z'})\sqrt{\frac{\sigma(e^+e^- \to \gamma Z'_{B-L})\mathrm{Br}(Z'_{B-L} \to \text{visible states})}{\sigma(e^+e^- \to \gamma Z')\mathrm{Br}(Z' \to \text{visible states})}}, \tag{49}$$

where Z'_{B-L} indicate Z' boson in the case of $U(1)_{B-L}$. The rescaling formula for the invisible Z' decay mode is

$$g_X^{\max}(M_{Z'}) = g_{B-L}^{\max}(M_{Z'})\sqrt{\frac{\sigma(e^+e^- \to \gamma Z'_{B-L})\mathrm{Br}(Z'_{B-L} \to \bar{\nu}\nu)}{\sigma(e^+e^- \to \gamma Z')\mathrm{Br}(Z' \to \bar{\nu}\nu)}}, \tag{50}$$

where all neutrino modes are taken into account.

F. Limits from electron and muon $(g-2)$

The Z' boson contributes to electron and muon $(g-2)$, $\Delta a_{\mu,e}$, at one-loop level. Calculating the one-loop diagram, we obtain the formula as [143]

$$\Delta a_\ell = \frac{g_X^2}{8\pi^2}\frac{m_\ell^2}{M_{Z'}^2}\int_0^1 dx \frac{(\tilde{x}_\ell + \tilde{x}_e)^2 2x^2(1-x) + (\tilde{x}_\ell - \tilde{x}_e)^2(2x(1-x)(x-4) - 4x^3\frac{m_\ell^2}{M_{Z'}^2})}{(1-x)(1-x\frac{m_\ell^2}{M_{Z'}^2}) + x\frac{m_\ell^2}{M_{Z'}^2}}, \tag{51}$$

where $\ell = \{e, \mu\}$. As a reference, we derive the region that accommodates experimental values of electron and muon $(g-2)$ in the models. For electron $(g-2)$, the experimentally obtained ranges are

$$\begin{aligned}\Delta a_e(^{133}\mathrm{Cs}) &= -(8.8 \pm 3.6) \times 10^{-13}, \\ \Delta a_e(^{87}\mathrm{Rb}) &= (4.8 \pm 3.0) \times 10^{-13},\end{aligned} \tag{52}$$

where the corresponding deviations from the SM are 2.4σ and 1.6σ, respectively [144,145]. We consider the Δa_e constraint on Z' interaction to satisfy either range of Δa_e depending on the charge assignment. For muon $(g-2)$ we apply the experimentally obtained range of [146]

$$\Delta a_\mu = (25.1 \pm 5.9) \times 10^{-10}, \tag{53}$$

which corresponds to 4.2σ deviation from the SM prediction. We show the parameter region that satisfies the Δa_μ range in the models.

IV. RESULTS AND DISCUSSIONS

We calculate the exclusion and future sensitivity regions for the chiral Z' gauge boson from neutrino-nucleon scattering measurements [FASER$\nu(2)$, SND@LHC], missing energy search (NA64), muon-electron scattering measurements (MUonE), proton and electron beam-dump experiments (Orsay, KEK, E137, CHARM, NOMAD, ν-cal, E141, E774, NA64), electron-neutrino scattering measurements (BOREXINO, TEXONO, JSNS2), coherent neutrino-nucleus scattering (COHERENT), and collider experiments (LEP-II, CMS, LHCb, *BABAR*). In Figs. 6–9, we show the exclusion and future sensitivity regions for $x_H = -2, -1, -0.5,\ 0,\ 0.5,\ 1,$ and 2 considering $x_\Phi = 1$ where the horizontal and vertical axes are Z' mass within the range $10^{-3} \le M_{Z'} \le 150$ GeV and gauge coupling constant g_X, respectively. The shaded regions have already been excluded, and on the other hand, the curves without shaded regions are sensitivity curves by future experiments. Along this line we compare the sensitivity lines from supernova (only in case of $x_H = -2$; bounds for other x_H can be found in [10]) and beam-dump experiments at FASER(2), DUNE, and ILC (ILC-BD) from [10]. The shaded regions in the figures are ruled out by respective experiments.

We show the prospective sensitivity in the g_X–$M_{Z'}$ plane obtained from the elastic $\mu^+ - e^-$ scattering at the MUonE experiment in the upper panel of Fig. 6 for $x_H = -2$ where left-handed fermions do not interact with the Z'. Bounds obtained from the MUonE experiment vary as $6 \times 10^{-4} \le g_X \le 0.4$ for $10^{-3} \le M_{Z'} \le 150$ GeV. It is found that MUonE bounds for $M_{Z'} \le 0.03$ GeV are ruled out by beam-dump searches from NA64 and E774, respectively, whereas these bounds for $M_{Z'} \ge 0.175$ GeV are ruled out by estimated limits obtained from the dark photon searches at *BABAR*, LHCb, CMS (CMS Dark), except for a narrow window from the LHCb experiment around $M_{Z'} \simeq 1$ GeV. Limits obtained from the electron magnetic dipole moment for Cesium-133 is stronger than the limits obtained from $\mu - e$ scattering at MUonE for $0.0174 \le M_{Z'} \le 0.0894$ GeV with $1.4 \times 10^{-4} \le g_X \le 7.16 \times 10^{-4}$. Following the analysis given in [10], we find that prospective sensitivity from the beam-dump experiments at FASER(2) can reach up to 5×10^{-3} at $M_{Z'} = 10^{-3}$ GeV, whereas ILC-BD reaches up to 2.5×10^{-3} at that $M_{Z'}$. However, these bounds are ruled out by the results from different beam-dump searches from NA64, E774, and E141, whereas the prospective reach

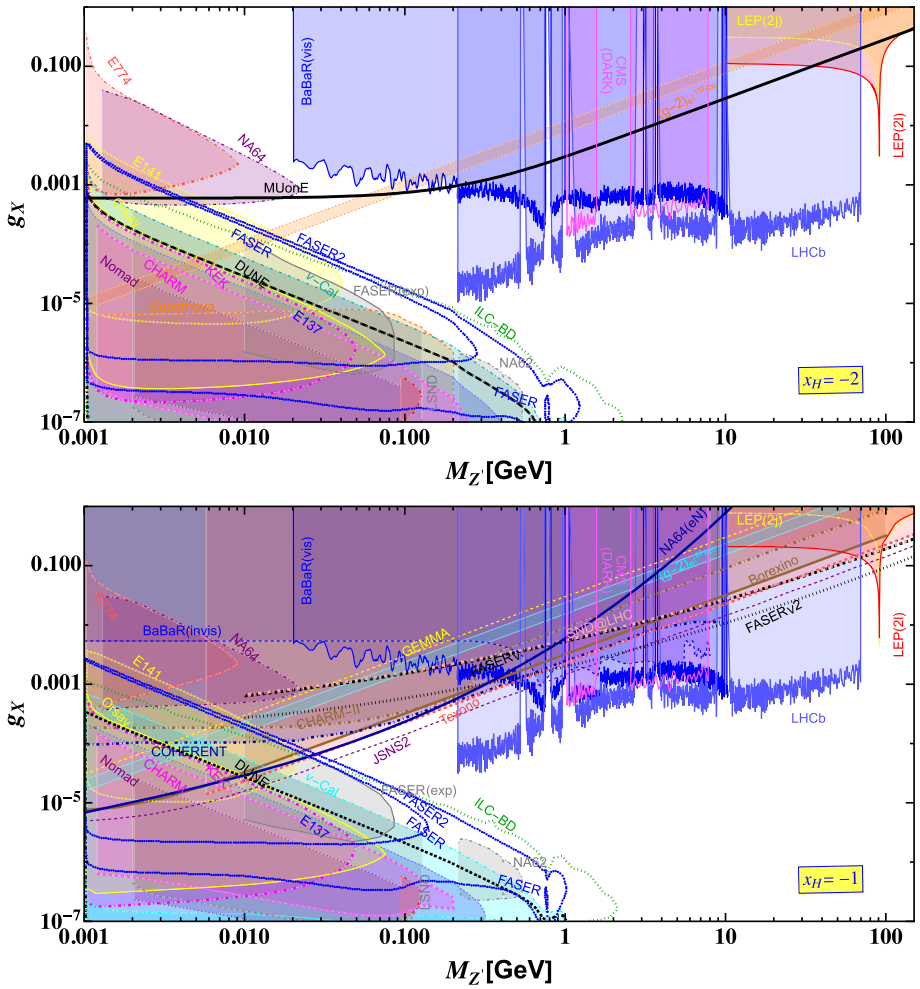

FIG. 6. Limits on g_X–$M_{Z'}$ plane for $x_H = -2$ [upper, $U(1)_R$ case] and $x_H = -1$ (lower) taking $x_\Phi = 1$ considering $10^{-3} \leq M_{Z'} \leq 150$ GeV. For $x_H = -2$ we show the region sensitive to the MUonE experiment. Recasting the data we compare the parameter region with those we estimated from LEP, dark photon searches at *BABAR*, LHCb, and CMS (CMS Dark), and different beam-dump experiments at Orsay, KEK, E137, CHARM, NOMAD, ν-cal, E141, E774, NA64, NA62, FASER, and involving prospective bounds from FASER(2), DUNE, and ILC-BD, respectively, from theoretical analyses. For $x_H = -1$ we show the regions sensitive to FASERν, FASERν2, SND@LHC, NA64(eN), and JSNS2 experiments. We compare our results recasting limits from LEP, CHARM-II, GEMMA, BOREXINO, COHERENT, TEXONO, dark photon search at *BABAR* [visible (vis) and invisible (invis)], LHCb, and CMS (CMS Dark), and different beam-dump experiments at Orsay, KEK, E137, CHARM, NOMAD, ν-cal, E141, E774, NA64, and involving prospective bounds from FASER(2), DUNE, and ILC, respectively. In this case, the MUonE bound cannot be calculated because e_R does not interact with the Z'.

from FASER(2) and ILC-BD can be improved for $M_{Z'} \simeq 0.3$ GeV. Following the analysis in [10], we find that supernova bounds can be slightly stronger than the ν-cal bounds around $M_{Z'} \simeq 0.1$ GeV. Within $10^{-3} \leq M_{Z'} \leq 0.18$ GeV the prospective bounds from DUNE (prospective DUNE sensitivity plots can be found in [10] for $0.1 \leq M_{Z'} \leq 3$ GeV) are weaker than ν-cal. We find that recent experimental observations from FASER (FASER-exp) [127] and NA62 [128] are represented by gray solid and dot-dashed lines and the corresponding excluded regions are shaded in gray. Most of these limits are well within the ν-cal bounds, however, the rest of them are just above the ν-cal contour, offering stronger constraints around $0.04 \leq M_{Z'} \leq 0.07$ GeV from FASER-exp and $0.25 \leq M_{Z'} \leq 0.55$ GeV from the NA62 experiment. The experimental limits from the FASER experiment (FASER-exp) are weaker than the theoretically estimated lines for the FASER experiment represented by blue dotted contour for $M_{Z'} > 0.04$ GeV. Recasting *BABAR*(vis) data for dark photon searches, we obtain a stringent bound for $M_{Z'} \leq 0.175$ GeV. Recasting the dark photon searches at the LHCb and CMS experiments, we find that stringent bounds can be calculated for $0.175 \leq M_{Z'} \leq 70$ and $1 \leq M_{Z'} \leq 8$ GeV, respectively. Except for small windows in these ranges where $M_{Z'} \simeq 10$ GeV, stringent bounds can be obtained from the visible final state in the *BABAR*(vis)

experiment. For $M_{Z'} \leq 0.19$ GeV, we compare our results recasting the limits from different beam-dump experiments including NOMAD, CHARM, KEK, E774, E141, E137, and ν-cal experiments with the prospective limits obtained from FASER(2), DUNE, and ILC-BD. Furthermore, dilepton and dijet searches also rule out the bounds for $M_{Z'} \geq 70$ GeV. We also show the dilepton and dijet limits when $M_{Z'}$ is at the Z pole giving a bound about 3×10^{-3} when $x_H = -2$. Because of the structure of the $U(1)_R$ scenario where left-handed fermions do not interact with the Z', we find no other constraints in this scenario from experiments like ν-electron, ν-nucleon, etc., where we cannot explore the coupling between ν_L and Z'.

Limits for $x_H = -1$ are shown in the lower panel of Fig. 6. For this charge, there is no coupling between e_R and Z' resulting in no direct bound from $\mu^+ - e^-$ scattering at the MUonE experiment. However, for this value of x_H, we obtain prospective limits from FASERν(2), SND@LHC, and ν-nucleus scattering at NA64 [NA64(eN)] where we compare recasting the bounds from the existing scattering experiments like GEMMA, BOREXINO, CHARM-II, TEXONO, and COHERENT. Bounds obtained from the TEXONO and COHERENT experiments are stronger than the other bounds obtained from the existing scattering experiments for the Z' roughly within $0.03 \leq M_{Z'} \leq 0.1$ GeV. The prospective bounds on the $U(1)_X$ gauge coupling varies within $7 \times 10^{-6} \leq g_X \leq 1$ from the electron-nucleon scattering process in the NA64(eN) experiment for $10^{-3} \leq M_{Z'} \leq 10$ GeV. However, the bound is comparable with the bounds obtained from the TEXONO and COHERENT experiments for the Z' mass within $0.03 \leq M_{Z'} \leq 0.1$ GeV; whereas bounds obtained from the NA64(eN) experiment are weak compared to the beam-dump experiments for $M_{Z'} \leq 0.028$ GeV. Here we recast existing results from different beam-dump experiments like Orsay, KEK, E137, CHARM, NOMAD, ν-cal, E141, E774, and NA64 for $x_H = -1$ to show complementarity with the other experiments. Prospective bounds on the $U(1)_X$ gauge coupling obtained from the beam-dump experiments like FASER(2) and ILC-BD could be stringent compared to the estimated bounds from the existing beam-dump experiments for $M_{Z'} \geq 0.2$ GeV. Interestingly the NA64(eN) line crosses ILC-BD and FASER2 lines at this mass point. With prospective limits obtained by performing the beam-dump study at DUNE, we obtain that those limits are weaker than the limits obtained by recasting the existing results from the ν-cal experiment. We find that recent experimental observations from FASER (FASER-exp) [127] and NA62 [128] are represented by gray solid and dot-dashed lines and the corresponding excluded regions are shaded in gray. Most of these limits are well within the ν-cal bounds, however, the rest of them are just above the ν-cal contour, offering stronger constraints around $0.0225 \leq M_{Z'} \leq 0.08$ GeV from FASER-exp and $0.25 \leq M_{Z'} \leq 0.55$ GeV from the NA62 experiment, respectively. The FASER-exp contour almost covers the theoretical region shown by the blue dotted line for the FASER experiment for $M_{Z'} > 0.07$ GeV. Estimated prospective bounds obtained from ν-nucleon scattering at FASERν and SND@LHC vary as $6.69 \times 10^{-4} \leq g_X \leq 0.29$ and those in the case of FASERν2 vary as $2.8 \times 10^{-4} \leq g_X \leq 0.14$ for $0.01 \leq M_{Z'} \leq 150$ GeV, respectively, showing stronger prospective bounds for $91.2 \leq M_{Z'} \leq 150$ GeV. We recast dilepton and dijet results from LEP, which provide the most stringent limit as $g_X \simeq 5 \times 10^{-3}$ at the Z pole. We recast recent results of dark photon searches at the LHCb and CMS providing constraints for $0.2 \leq M_{Z'} \leq 70$ and $1 \leq M_{Z'} \leq 8$ GeV, respectively. Constraints on g_X from LHCb vary as $3.12 \times 10^{-5} \leq g_X \leq 1.09 \times 10^{-3}$ and those from CMS Dark vary as $4.0 \times 10^{-4} \leq g_X \leq 1.1 \times 10^{-3}$, leaving some narrow windows where *BABAR*(vis) provides the strongest bound around $M_{Z'} \simeq 10$ GeV as $g_X \simeq 7 \times 10^{-4}$. Studying ν-electron scattering at JSNS2, we find that a prospective sensitivity for g_X could reach as low as 2.78×10^{-5} and as high as 3×10^{-3} for $M_{Z'} = 0.022$ and 0.22 GeV, respectively, which could be probed in the future. JSNS2 provides stronger bounds for $M_{Z'}$ above the Z pole. Recasting the data from the different beam-dump experiments, we find that prospective bounds obtained from JSNS2 could be weaker than some of these bounds for $M_{Z'} \leq 0.025$ GeV. In addition to that, we estimate bounds on the $U(1)_X$ coupling analyzing the electron $g-2$ data, which belong to the shaded region being ruled out by the scattering, dark photon search, and beam-dump experiments.

Limits for $x_H = -0.5$ are shown in the upper panel of Fig. 7. In this case, u_R does not interact with the Z'. We obtain the prospective sensitivity on g_X by estimating the $\mu^- - e^+$ scattering process involving the Z' contribution at the MUonE experiment. Estimated limits are weaker than the projected sensitivities obtained from the ν-nucleon scattering at the experiments like FASERν and SND@LHC except for $M_{Z'} \leq 0.73$ GeV. Studying ν-nucleon scattering for the FASERν2 experiment, we find that the prospective sensitivities could be stronger than the projections of FASERν, SND@LHC, and MUonE experiments. The prospective limit obtained from the FASERν2 experiment could reach $g_X \simeq 0.15$ for $M_{Z'}$ going beyond the Z pole. At the Z pole, we recast dilepton and dijet bounds from the LEP experiment and find that the exclusion limit on the coupling could reach $g_X \simeq 3 \times 10^{-3}$. Limits estimated by recasting the COHERENT ν-nucleus scattering are obtained to be strong for $0.066 \leq M_{Z'} \leq 0.213$ GeV, where coupling varies as $9.0 \times 10^{-5} \leq g_X \leq 2.36 \times 10^{-4}$. We find that COHERENT limits are weaker than the limits obtained by the e-nucleus scattering at the NA64 experiment [NA64(eN)] for $M_{Z'} \leq 0.07$ GeV, while NA64(eN) limits are weaker than the those from COHERENT, TEXONO, and BOREXINO experiments beyond this $M_{Z'}$. Recasting the dark photon searches at the experiments like *BABAR*, LHCb, and CMS, we find that stringent limits come from LHCb within $0.21 \leq M_{Z'} \leq 70$ GeV, whereas those from *BABAR*

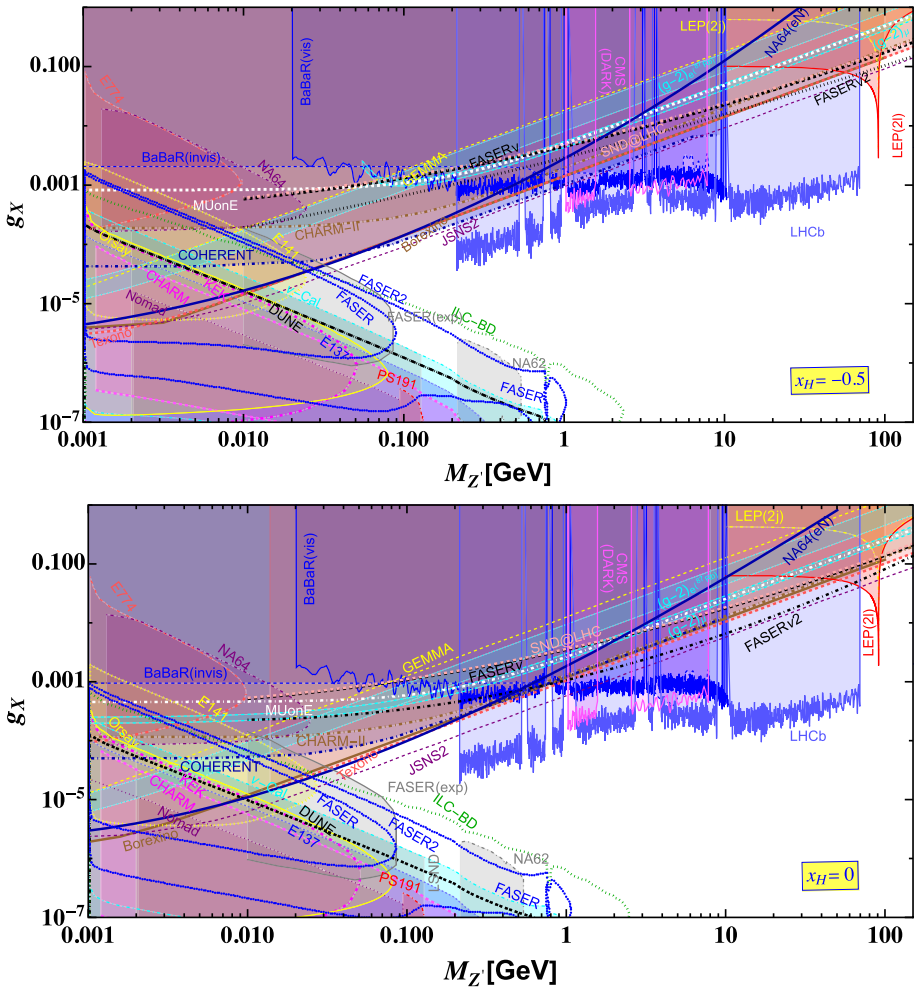

FIG. 7. Limits on g_X–$M_{Z'}$ plane for $x_H = -0.5$ (upper) and $x_H = 0$ (lower, $B-L$ case) taking $x_\Phi = 1$ considering $10^{-3} \leq M_{Z'} \leq 150$ GeV, showing the regions sensitive to FASERν, FASERν2, SND@LHC, NA64(eN), and JSNS2 experiments. Recasting the existing results in our case, we compare parameter regions obtained from LEP, dark photon searches at *BABAR* (vis and invis), LHCb, and CMS(CMS Dark), scattering experiments CHARM-II, GEMMA, BOREXINO, COHERENT, TEXONO, and different beam-dump experiments from Orsay, KEK, E137, CHARM, NOMAD, ν-cal, E141, E774, NA64, NA62, FASER involving prospective bounds from FASER(2), DUNE, and ILC(ILC-BD), respectively, from theoretical analyses.

(vis) could have severe bounds around $M_{Z'} \simeq 10$ GeV and CMS Dark could have severe bounds around $M_{Z'} \simeq 1$ and 3 GeV. We obtain prospective sensitivity from the JSNS2 experiment studying ν-electron scattering where the most stringent bound comes within the range $0.024 \leq M_{Z'} \leq 0.215$ GeV, where the $U(1)_X$ gauge coupling varies within $2.46 \times 10^{-5} \leq g_X \leq 1.97 \times 10^{-4}$. JSNS2 could also produce a stringent prospective bound on g_X for $M_{Z'}$ beyond the Z pole that is close to the prospective limit from FASERν2 for $M_{Z'} \simeq 150$ GeV. The prospective sensitivity line from JSNS2 crosses over the bounds obtained from the prospective limits from the beam-dump scenarios like FASER at $M_{Z'} = 0.0287$ GeV, whereas FASER2 and ILC-BD lines at $M_{Z'} = 0.0326$ GeV and the corresponding couplings are 2.8×10^{-5} and 3.21×10^{-5}, respectively. We find that recent experimental observations from FASER (FASER-exp) [127] and NA62 [128] are represented by gray solid and dot-dashed lines and the corresponding excluded regions are shaded in gray. Some parts of these limits are well within the ν-cal bounds; however, the rest of them are above the ν-cal contour, offering stronger constraints around $0.03 \leq M_{Z'} \leq 0.09$ GeV from FASER-exp and $0.225 \leq M_{Z'} \leq 0.5$ GeV from the NA62 experiment, respectively. The FASER-exp contour almost covers the theoretical region shown by the blue dotted line for $x_H = -0.5$. Recasting the data obtained from the existing results of E774, E137, E141, NA64, Orsay, KEK, NOMAD, and ν-cal, we find that prospective bounds obtained from DUNE for $M_{Z'} \leq 0.15$ GeV are weaker than the bounds obtained from recasting the data of the ν-cal experiment. We estimated bounds on g_X from the electron and muon $g-2$ data. However, the limits are weaker compared to different existing and prospective scattering and dark photon experiments mentioned for this charge. Similar behavior is

seen for the sensitivity line obtained after recasting the data from the GEMMA experiment, which is weak compared to existing beam-dump, scattering, and dark photon searches.

We estimate limits on g_X for $x_H = 0$ depending on $M_{Z'}$ in the lower panel of Fig. 7. We mention that $x_H = 0$ is the well-known $B - L$ scenario. We estimate prospective limits at experiments like MUonE, FASER$\nu(2)$, and SND@LHC and find that these sensitivities belong to the shaded region below the Z pole. However, above the Z pole, the prospective limits from FASERν2 become stringent for $M_{Z'} \leq 150$ GeV, the range of Z' mass under consideration. Recasting the dilepton and dijet search results from LEP, we find the strongest bound at the Z pole to be 0.0018. Recasting available data, we find that limits obtained from GEMMA, CHARM-II, and COHERENT also belong to the shaded region, being weak compared to the bounds from different scattering experiments involving TEXONO and BOREXINO, beam-dump experiments involving E774, E131, E141, NA64, Orsay, KEK, NOMAD, and ν-cal, CHARM and dark photon search experiments involving *BABAR* (visible and invisible modes), LHCb, and CMS after we recast the available data from these experiments. We calculate prospective limits from e-nucleon scattering at the NA64 experiment that are slightly stronger than existing bounds obtained from the TEXONO experiment for $0.02 \leq M_{Z'} \leq 0.164$ GeV, where limits on the $U(1)_X$ coupling can reach up to $2.0 \times 10^{-5} \leq g_X \leq 7.2 \times 10^{-4}$. We show bounds obtained from the dark photon search experiments at *BABAR* (visible and invisible), LHCb, and CMS and found that LHCb provides a strong bound on the $U(1)_X$ gauge coupling for $0.21 \leq M_{Z'} \leq 70$ GeV, whereas for narrow windows around $M_{Z'} \simeq 10$ GeV, limits obtained from *BABAR* are stringent and limits on g_X are stringent around $M_{Z'} \simeq 1$ and 3 GeV from CMS Dark, respectively. Prospective bounds from the JSNS2 experiment could be stronger than the other scattering experiments for $0.028 \leq M_{Z'} \leq 0.21$ GeV, where constraints on the $U(1)_X$ coupling constant could be as strong as $1.7 \times 10^{-5} \leq g_X \leq 1.3 \times 10^{-4}$. Starting from beyond the Z pole, the prospective search reach from JSNS2 could be around $g_X = 0.02$ for $M_{Z'} \leq 150$ GeV. We compare our results with different prospective beam-dump scenarios at DUNE, FASER (2), and ILC-BD. Doing that, we find that prospective reach from JSNS2 could intersect the prospective beam-dump lines from FASER(2) and ILC-BD at $\{M_{Z'}, g_X\} = \{0.025\,\text{GeV}, 1.55 \times 10^{-5}\}, \{0.032\,\text{GeV}, 1.92 \times 10^{-5}\}, \{0.035\,\text{GeV}, 2.13 \times 10^{-5}\}$, respectively, which could be probed in the near future. Prospective limits obtained from DUNE are weaker than the ν-cal bounds for $M_{Z'} \leq 0.08$ GeV. We find that recent experimental observations from FASER (FASER-exp) [127] and NA62 [128] are represented by gray solid and dot-dashed lines and the corresponding excluded regions are shaded in gray. Some parts of these limits are well within the ν-cal bounds, however, the rest of them are above the ν-cal contour, offering stronger constraints around $0.03 \leq M_{Z'} \leq 0.08$ GeV from FASER-exp and $0.225 \leq M_{Z'} \leq 0.5$ GeV from the NA62 experiment, respectively. The FASER-exp contour covers the theoretical region shown by the blue dotted line for $0.01 \leq M_{Z'} \leq 0.085$ GeV, however, these are stronger than the theoretical limits.

The limits on the g_X–$M_{Z'}$ plane for $x_H = 0.5$ has been shown in the upper panel of Fig. 8, where all the fermions interact with the Z', however, left- and right-handed interactions with the Z' are different. We estimate prospective limits from the $\mu^+ - e^-$ scattering at the MUonE experiment and compare it with the bounds recasting the data from other scattering experiment involving GEMMA, TEXONO, BOREXINO, CHARM-II, and COHERENT. We find that bounds from TEXONO rule out the other results. We also estimate the bounds from the prospective search reaches at the experiments involving SND@LHC and FASER$\nu(2)$. We find that FASERν2 could provide a stringent limit beyond the Z pole up to $M_{Z'} \leq 150$ GeV, where constraints on g_X could reach around 0.1. Using the dilepton and dijet searches from LEP, we recast those data in our scenario to obtain a strong limit on $M_{Z'}$ at the Z pole as $g_X = 0.0012$. We find that electron-nucleon scattering in NA64(eN) gives a strong bound on the $U(1)_X$ coupling as $2.22 \times 10^{-5} \leq g_X \leq 1.17 \times 10^{-4}$ for the Z' within $0.028 \leq M_{Z'} \leq 0.14$ GeV, which is slightly stronger than the bounds obtained from TEXONO and COHERENT within that range of $M_{Z'}$. We calculate bounds on g_X recasting the data obtained from the dark photon searches at *BABAR*, LHCb, and CMS, respectively. Hence we find that LHCb provides a stringent bound for the Z' mass within $0.21 \leq M_{Z'} \leq 70$ GeV, where limits on g_X vary within $10^{-5} \leq g_X \leq 2 \times 10^{-4}$, and around $M_{Z'} \simeq 10$ GeV *BABAR* provides stringent constraints, whereas around $M_{Z'} \simeq 1$ and 3 GeV CMS Dark provides stringent constraints on the $U(1)_X$ gauge coupling. We study $\nu - e$ scattering for the JSNS2 experiment. JSNS2 shows prospective strongest bounds compared to other scattering experiments and dark photon searches within $0.031 \leq M_{Z'} \leq 0.21$ GeV where limits on the coupling vary as $1.32 \times 10^{-5} \leq g_X \leq 9.1 \times 10^{-5}$. Following the JSNS2 line, we find that it may provide a strong bound on g_X beyond the Z pole which might reach up to $g_X \simeq 0.06$ for $M_{Z'} \leq 150$ GeV. Limits on g_X calculating electron and muon $g - 2$ scenarios are found to be weak compared to the existing scattering, beam-dump, and dark photon search experiments. Recasting the data from the beam-dump experiments involving NA64, E141, E137, CHARM, NOMAD, ν-cal, and KEK, we find the limits on the g_X–$M_{Z'}$ plane shown by the shaded areas. We find that recent experimental observations from FASER (FASER-exp) [127] and NA62 [128] are represented by gray solid and dot-dashed lines and the corresponding excluded regions are shaded in gray. Some parts of these limits are well within the ν-cal bounds, however, the rest of them are above the ν-cal contour offering stronger constraints

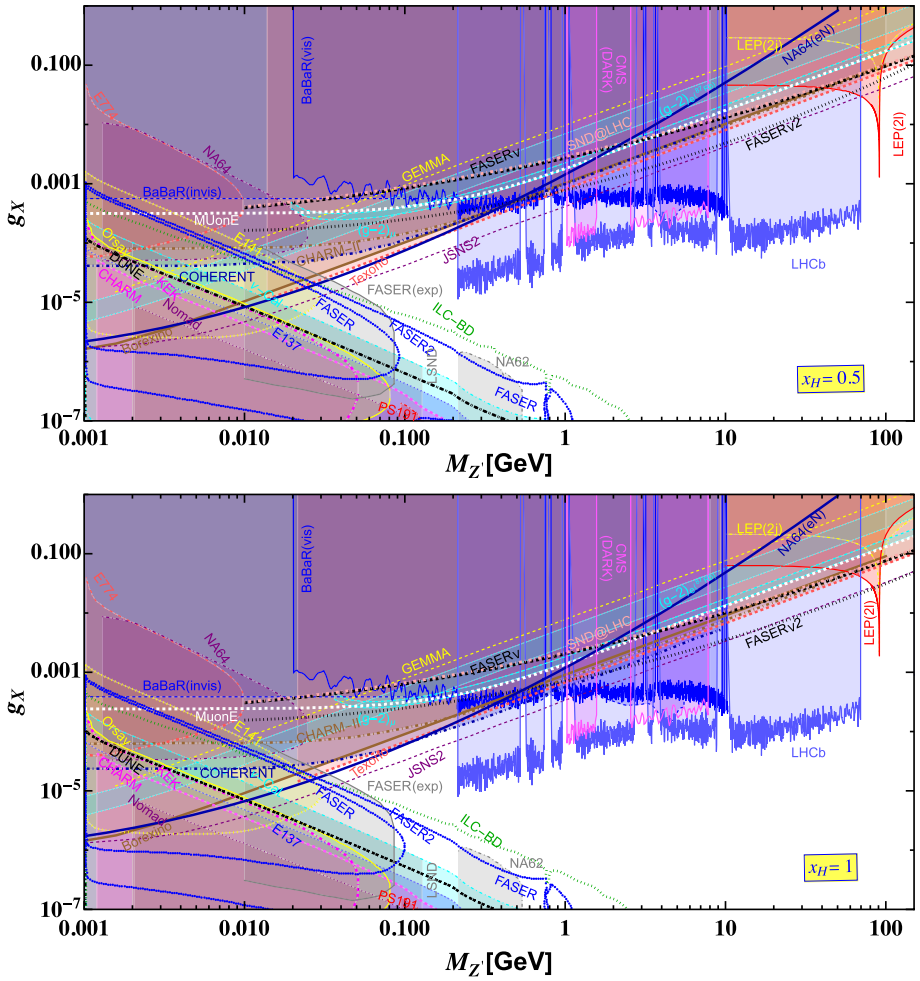

FIG. 8. Limits on g_X–$M_{Z'}$ plane for $x_H = 0.5$ (upper) and $x_H = 1$(lower) taking $x_\Phi = 1$ considering $10^{-3} \leq M_{Z'} \leq 150$ GeV showing the regions sensitive to FASERν, FASERν2, SND@LHC, NA64(eN), and JSNS2 experiments. Recasting the existing results in our case, we compare parameter regions obtained from scattering experiments at LEP, CHARM-II, GEMMA, BOREXINO, COHERENT, TEXONO, dark photon searches at *BABAR* (vis and invis), LHCb, and CMS(CMS Dark) experiments, and different beam-dump experiments at Orsay, KEK, E137, CHARM, NOMAD, ν-cal, E141, E774, NA64, NA62, FASER involving prospective theoretical bounds from FASER(2), DUNE, and ILC(ILC-BD), respectively.

around $0.035 \leq M_{Z'} \leq 0.09$ GeV from FASER-exp and $0.225 \leq M_{Z'} \leq 0.525$ GeV from the NA62 experiment. We also show the prospective sensitivities from FASER (2), DUNE, and ILC-BD, where sensitivity from DUNE is weaker compared to ν-cal for $M_{Z'} \leq 0.08$ GeV. The prospective sensitivity line from JSNS2 crosses the prospective FASER, FASER2, and ILC-BD lines at $\{M_{Z'}, g_X\} = \{0.0305\ \text{GeV}, 1.29 \times 10^{-5}\}$, $\{0.035\ \text{GeV}, 1.54 \times 10^{-5}\}$, $\{0.0374\ \text{GeV}, 1.65 \times 10^{-5}\}$, respectively. These limits could be probed by the scattering and beam-dump experiments in the future.

In the lower panel of Fig. 8, we show the constraints on the general $U(1)_X$ coupling for different $M_{Z'}$ using $x_H = 1$, where d_R does not interact with the Z'. We estimate prospective limits from $\mu^+ - e^-$ scattering at the MUonE experiment and compare it with the bounds recasting the results from CHARM-II, TEXONO, BOREXINO, GEMMA, and COHERENT experiments. We find that comparing with all these limits MUonE is weak, staying in the shaded region for $10^{-3} \leq M_{Z'} \leq 150$ GeV. Prospective sensitivity obtained from the electron-nucleon scattering at the NA64 experiment is denoted by the NA64(eN) line. This provides the strongest prospective limit within $0.0257 \leq M_{Z'} \leq 0.0085$ GeV, where $U(1)_X$ coupling could reach down to $1.423 \times 10^{-5} \leq g_X \leq 10^{-5}$. Recasting the TEXONO data, we find that in this context strong constraints come for $0.0254 \leq M_{Z'} \leq 0.072$ GeV, where limits on the gauge coupling vary within $1.72 \times 10^{-5} \leq g_X \leq 4.64 \times 10^{-5}$. We find that bounds obtained from TEXONO can be stronger than the limits obtained from recasting the dilepton and dijet searches at the LEP experiment beyond the Z pole but $M_{Z'} \leq 150$ GeV where limits on the gauge coupling could vary within $0.031 \leq g_X \leq 0.051$. In addition, we obtain that LEP bounds at the Z pole could reach

$g_X \simeq 0.0019$ from the dilepton and dijet searches. FASERν2 provides a prospective sensitivity beyond the Z pole and below 150 GeV, where limits could vary within $0.03 \leq g_X \leq 0.05$. The fermions in the $U(1)_X$ scenario under consideration interact equally with the Z', making a generation-independent nature of the model irrespective of x_H, which affects bounds from the $g-2$ analysis. This is true for any value of x_H. We find that limits obtained from the dark photon searches at LHCb show the strongest bounds on the $U(1)_X$ gauge coupling within $8.41 \times 10^{-6} \leq g_X \leq 1.637 \times 10^{-4}$ for $0.21 \leq M_{Z'} \leq 70$ GeV. We find that the dark photon search at CMS provides the strongest bounds on the gauge coupling for $M_{Z'}$ around 1 and 3 GeV, whereas the same scenario appears from the *BABAR* experiment for $M_{Z'}$ around 10 GeV. Prospective limits estimated in the context of the JSNS2 experiment are found to reach $1.85 \times 10^{-4} \leq g_X \leq 1.95 \times 10^{-4}$ for $0.517 \leq M_{Z'} \leq 0.56$ GeV, and beyond the Z pole, the bounds are comparable with the prospective ones from FASERν2. We find that recent experimental observations from FASER (FASER-exp) [127] and NA62 [128] are represented by gray solid and dot-dashed lines and the corresponding excluded regions are shaded in gray. Some parts of these limits are well within the ν-cal bounds, however, the rest of them are above the ν-cal contour, offering stronger constraints around $0.035 \leq M_{Z'} \leq 0.09$ GeV from FASER-exp and $0.225 \leq M_{Z'} \leq 0.525$ GeV from the NA62 experiment. Prospective limits from JSNS2 cross the prospective sensitivity lines at the beam-dump experiments involving FASER, FASER2, and ILC-BD at $\{M_{Z'}, g_X\} = \{0.033 \text{ GeV}, 1.05 \times 10^{-5}\}$, $\{0.036 \text{ GeV}, 1.21 \times 10^{-5}\}$, $\{0.0375 \text{ GeV}, 1.30 \times 10^{-5}\}$, respectively, which could be probed in the future. We compare these bounds by recasting the data from different beam-dump experiments like E141, NA64, KEK, Orsay, CHARM, E137, and ν-cal, which are shown by different shaded regions. We find that prospective bounds obtained from DUNE are weaker than ν-cal for $M_{Z'} \leq 0.06$ GeV.

We show the bounds from different experiments for $x_H = 2$ in Fig. 9. This charge is another example where all fermions interact with the Z', however, their left- and right-handed counterparts interact differently with the Z'. Being influenced by the charge assignment, we find that prospective bounds on g_X for different $M_{Z'}$ obtained from the MUonE experiment are weaker compared to the bounds after recasting the data from the TEXONO, BOREXINO, CHARM-II, and COHERENT experiments. We estimate prospective bounds on g_X for different prospective experiments like SND@LHC and FASERν(2). We find that prospective searches from FASERν2 are strong only beyond the Z pole and up to $M_{Z'} \leq 150$ GeV. In this mass range, the limits on g_X vary within $0.014 \leq g_X \leq 0.025$. Recasting the dilepton and dijet searches from the LEP experiment, we find that the limit on g_X at the Z pole could be as stringent as 6.8×10^{-4}. We also find that electron-nucleon scattering in the NA64 experiment shown by the line NA64(eN) provides a strong bound on the gauge coupling around $1.1 \times 10^{-5} \leq g_X \leq 1.1 \times 10^{-4}$ for $0.0261 \leq M_{Z'} \leq 0.21$ GeV. Studying ν-electron scattering in the context of the JSNS2 experiment, we estimate the prospective bounds on g_X with respect to $M_{Z'}$. The strongest future limits on g_X can be estimated for Z' within $0.032 \leq M_{Z'} \leq 0.212$ GeV as $7.735 \times 10^{-6} \leq g_X \leq 5.13 \times 10^{-5}$, which crosses respective future sensitivity lines obtained

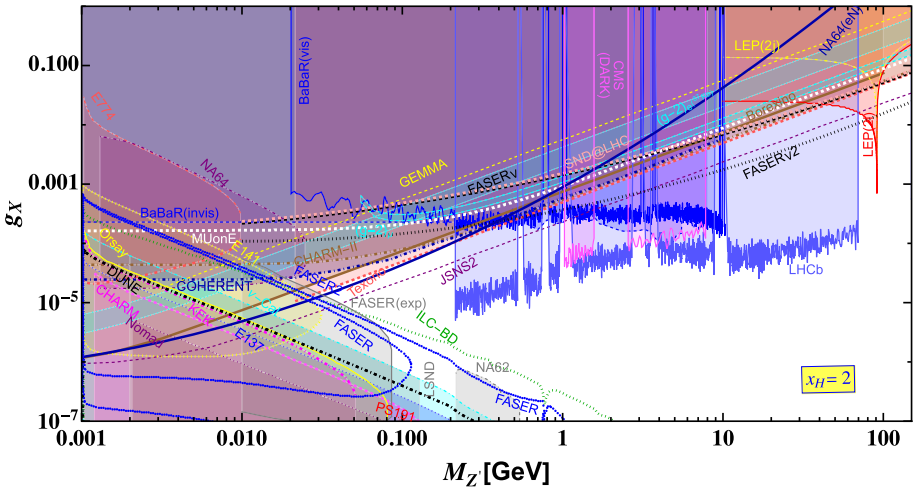

FIG. 9. Limits on g_X–$M_{Z'}$ plane for $x_H = 2$ taking $x_\Phi = 1$ considering $10^{-3} \leq M_{Z'} \leq 150$ GeV, showing the regions sensitive to FASERν, FASERν2, SND@LHC, NA64(eN), and JSNS2 experiments. Recasting the existing results in our case, we compare parameter regions obtained from the scattering experiments at LEP, CHARM-II, GEMMA, BOREXINO, COHERENT, TEXONO, dark photon searches at *BABAR* (vis and invis), LHCb, and CMS(CMS Dark), and different beam-dump experiments at Orsay, KEK, E137, CHARM, NOMAD, ν-cal, E141, E774, NA64, NA62, and FASER, and involving prospective bounds from FASER(2), DUNE, and ILC (ILC-BD), respectively.

from the beam-dump experiments like FASER, FASER2, and ILC-BD at $\{M_{Z'}, g_X\} = \{0.033\,\text{GeV}, 7.855 \times 10^{-6}\}$, $\{0.0371\,\text{GeV}, 8.57 \times 10^{-6}\}$, and $\{0.0386\,\text{GeV}, 9.07 \times 10^{-6}\}$ that could be probed in the future. We compare our results for $x_H = 2$, recasting the bounds obtained from the existing results from the beam-dump experiments like E141, NA64, KEK, Orsay, CHARM, E137, and ν-cal. The excluded regions are shown by different shades. We find that recent experimental observations from FASER (FASER-exp) [127] and NA62 [128] are represented by gray solid and dot-dashed lines and the corresponding excluded regions are shaded in gray. Some parts of these limits are well within the ν-cal bounds, however, the rest of them are above the ν-cal contour, offering stronger constraints around $0.035 \leq M_{Z'} \leq 0.095$ GeV from FASER-exp and $0.225 \leq M_{Z'} \leq 0.525$ GeV from the NA62 experiment. We find that prospective bounds obtained from the beam-dump scenario at DUNE for $M_{Z'} \leq 0.04$ GeV are weaker than those obtained from ν-cal experiment recasting the existing data. Dark photon searches from LHCb provide stronger limits for $0.21 \leq M_{Z'} \leq 70$ GeV and beyond the Z pole up to $M_{Z'} = 150$ GeV. We find that LHCb limits below the Z pole vary within $3.5 \times 10^{-6} \leq g_X \leq 10^{-4}$. Stringent limits can be obtained from the dark photon search experiments at *BABAR* and CMS Dark around $M_{Z'} \simeq 10$ and $M_{Z'} \simeq 1$ and 3 GeV within narrow windows from the LHCb experiment. Finally, we comment that limits obtained from muon and electron $g-2$ studies are weaker than the scattering and beam-dump experiments due to the generation-independent nature of the fermionic couplings with Z'.

V. CONCLUSIONS

In this paper, we consider chiral scenarios where Z' interacts with the left- and right-handed fermions differently. We obtain that, depending on $U(1)_X$ charges, the interactions of the fermions with the Z' get modified by manifesting the chiral nature of the scenarios under consideration. Such interactions affect Z' mediated neutrino-electron, electron-nucleon, and electron-muon scattering processes that could be probed at experiments like FASERν(2), SND@LHC, NA64(eN), MUonE, JSNS2 and dark photon searches at *BABAR*, LHCb, and CMS experiments, respectively. Furthermore, we compare our results with dilepton, dijet searches from LEP, neutrino-nucleus coherent scattering at the COHERENT experiment, and electron-neutrino scattering experiments like BOREXINO, TEXONO, GEMMA, and CHARM-II. We compare our results studying visible and invisible final states at the *BABAR* experiment. Finally, we show complementarity with different beam-dump experiments like ν-cal, E137, E141, NA64, E774, Orsay, CHARM, KEK, NOMAD, and future experiments like FASER, FASER2, and ILC-BD. We find that the experimental results from FASER matches the theoretical limits estimated for general $U(1)_X$ charges having some bounds stronger than our estimated ones for increasing $M_{Z'}$. We have also shown the NA62 regions that cover some prospective regions that could be probed by the FASER2 experiment in the future.

Analyzing different interactions, we find that some prospective bounds at NA64(eN), FASERν2, and JSNS2 could be probed in the future. Some of the existing experimental limits from LEP, TEXONO, *BABAR* (visible), and dark photon searches at LHCb and CMS show stringent upper limits on g_X for the respective Z' mass. JSNS2 bounds cross the future sensitivities estimated from FASER, FASER2, and ILC-BD, which could also be verified in the future; however, their crossovers depend on x_H, which could be checked after the realistic experimental results are available. Depending on the $U(1)_X$ charge, we find that beam-dump experiments like ν-cal, E137, E141, NA64, E774, Orsay, CHARM, KEK, and NOMAD rule out the values of $U(1)_X$ coupling within $10^{-6} \leq g_X \leq 0.01$ depending on the Z' mass for $M_{Z'} \leq 0.08$ GeV. Within the mass range of Z', we find that DUNE will provide a weaker bound from the beam-dump scenario. We find that weaker limits are obtained when analyzing the $g-2$ data because, in our model, three generations of the fermions are equally coupled with the Z'. We point out that limits from SND@LHC and FASERν are weak compared to the other scattering experiments below the Z pole. Finally, from our analysis it has been found that scattering experiments could probe lighter Z' within $0.02 \leq M_{Z'} \leq 0.2$ GeV, which could be simultaneously probed by proposed beam-dump experiments involving FASER, FASER2, and ILC-BD. We find that in the case of the $U(1)_R$ scenario, MUonE could provide a stringent bound for $0.02 \leq M_{Z'} \leq 0.175$ GeV. On the other hand, Z' above the Z pole but $M_{Z'} \leq 150$ GeV which could be probed by high-energy colliders experiments in the future for the cases we considered except $x_H = -2$. Hence we conclude that studying Z' mediated interactions in addition to the SM processes, limits on general $U(1)_X$ couplings could be interesting to probe the $\mathcal{G}_{\text{SM}} \otimes U(1)_X$ scenario in the future.

ACKNOWLEDGMENTS

We thank Takashi Shimomura and Yuichi Uesaka for useful advice. This work is supported by JSPS KAKENHI Grants No. JP21K20365 and No. JP23K13097 (K. A.), No. JP19K03860, No. JP19K03865, and No. JP23K03402 (O. S.), by the Fundamental Research Funds for the Central Universities (T. N. and J. L.), and the Natural Science Foundation of Sichuan Province under Grant No. 2023NSFSC1329 and the National Natural Science Foundation of China under Grant No. 11905149 (J. L.).

[1] Particle Data Group, Review of particle physics, Prog. Theor. Exp. Phys. **2020**, 083C01 (2020).

[2] G. Bertone, D. Hooper, and J. Silk, Particle dark matter: Evidence, candidates and constraints, Phys. Rep. **405**, 279 (2005).

[3] Planck Collaboration, Planck 2018 results. VI. Cosmological parameters, Astron. Astrophys. **641**, A6 (2020); **652**, C4(E) (2021).

[4] P. Minkowski, $\mu \to e\gamma$ at a rate of one out of 10^9 muon decays?, Phys. Lett. **67B**, 421 (1977).

[5] O. Sawada and A. Sugamoto, Horizontal gauge symmetry and masses of neutrinos, Conf. Proc. C **7902131**, 95 (1979).

[6] M. Gell-Mann, P. Ramond, and R. Slansky, Complex spinors and unified theories, Conf. Proc. C **790927**, 315 (1979).

[7] R. N. Mohapatra and G. Senjanovic, Neutrino mass and spontaneous parity nonconservation, Phys. Rev. Lett. **44**, 912 (1980).

[8] J. Schechter and J. W. F. Valle, Neutrino masses in $SU(2) \times U(1)$ theories, Phys. Rev. D **22**, 2227 (1980).

[9] S. Weinberg, Baryon and lepton nonconserving processes, Phys. Rev. Lett. **43**, 1566 (1979).

[10] K. Asai, A. Das, J. Li, T. Nomura, and O. Seto, Chiral Z' in FASER, FASER2, DUNE, and ILC beam dump experiments, Phys. Rev. D **106**, 095033 (2022).

[11] M. Bauer, P. Foldenauer, and J. Jaeckel, Hunting all the hidden photons, J. High Energy Phys. 07 (2018) 094.

[12] P. Ilten, Y. Soreq, M. Williams, and W. Xue, Serendipity in dark photon searches, J. High Energy Phys. 06 (2018) 004.

[13] P. S. B. Dev, B. Dutta, K. J. Kelly, R. N. Mohapatra, and Y. Zhang, Light, long-lived $B - L$ gauge and Higgs bosons at the DUNE near detector, J. High Energy Phys. 07 (2021) 166.

[14] C. Baruch, P. Ilten, Y. Soreq, and M. Williams, Axial vectors in DarkCast, J. High Energy Phys. 11 (2022) 124.

[15] A. Greljo, P. Stangl, A. E. Thomsen, and J. Zupan, On $(g-2)_\mu$ from gauged $U(1)_X$, J. High Energy Phys. 07 (2022) 098.

[16] N. Bernal and Y. Farzan, Neutrino nonstandard interactions with arbitrary couplings to u and d quarks, Phys. Rev. D **107**, 035007 (2023).

[17] A. Boyarsky, O. Mikulenko, M. Ovchynnikov, and L. Shchutska, Searches for new physics at SND@LHC, J. High Energy Phys. 03 (2022) 006.

[18] S. Ansarifard and Y. Farzan, Neutral exotica at FASERν and SND@LHC, J. High Energy Phys. 02 (2022) 049.

[19] A. Aboubrahim, M. M. Altakach, M. Klasen, P. Nath, and Z.-Y. Wang, Combined constraints on dark photons and discovery prospects at the LHC and the forward physics facility, J. High Energy Phys. 03 (2023) 182.

[20] F. Kling, J.-L. Kuo, S. Trojanowski, and Y.-D. Tsai, FLArE up dark sectors with EM form factors at the LHC forward physics facility, Nucl. Phys. **B987**, 116103 (2023).

[21] K. J. Kelly, P. A. N. Machado, A. Marchionni, and Y. F. Perez-Gonzalez, LEvEL: Low-energy neutrino experiment at the LHC, J. High Energy Phys. 08 (2021) 087.

[22] P. S. B. Dev, D. Kim, K. Sinha, and Y. Zhang, New interference effects from light gauge bosons in neutrino-electron scattering, Phys. Rev. D **104**, 075001 (2021).

[23] G. Chauhan, P. S. B. Dev, and X.-J. Xu, Probing the ν_R-philic Z' at DUNE near detectors, Phys. Lett. B **841**, 137907 (2023).

[24] R. Coy and X.-J. Xu, Probing the muon $g-2$ with future beam dump experiments, J. High Energy Phys. 10 (2021) 189.

[25] A. L. Foguel, G. M. Salla, and R. Z. Funchal, (In)Visible signatures of the minimal dark Abelian gauge sector, J. High Energy Phys. 12 (2022) 063.

[26] M. D. Campos, D. Cogollo, M. Lindner, T. Melo, F. S. Queiroz, and W. Rodejohann, Neutrino masses and absence of flavor changing interactions in the 2HDM from gauge principles, J. High Energy Phys. 08 (2017) 092.

[27] M. Lindner, F. S. Queiroz, W. Rodejohann, and X.-J. Xu, Neutrino-electron scattering: General constraints on Z' and dark photon models, J. High Energy Phys. 05 (2018) 098.

[28] M. Atzori Corona, M. Cadeddu, N. Cargioli, F. Dordei, C. Giunti, Y. F. Li, E. Picciau, C. A. Ternes, and Y. Y. Zhang, Probing light mediators and $(g-2)_\mu$ through detection of coherent elastic neutrino nucleus scattering at COHERENT, J. High Energy Phys. 05 (2022) 109.

[29] K. Chakraborty, A. Das, S. Goswami, and S. Roy, Constraining general U(1) interactions from neutrino-electron scattering measurements at DUNE near detector, J. High Energy Phys. 04 (2022) 008.

[30] A. Ismail, R. Mammen Abraham, and F. Kling, Neutral current neutrino interactions at FASERν, Phys. Rev. D **103**, 056014 (2021).

[31] P. Bakhti, Y. Farzan, and S. Pascoli, Discovery potential of FASERν with contained vertex and through-going events, J. High Energy Phys. 04 (2021) 075.

[32] K. Cheung and C. J. Ouseph, Sensitivities on dark photon from the forward physics experiments, J. High Energy Phys. 10 (2022) 196.

[33] K. Cheung, C. J. Ouseph, and T. Wang, Non-standard neutrino and Z' interactions at the FASERν and the LHC, J. High Energy Phys. 12 (2021) 209.

[34] P. Bakhti, Y. Farzan, and S. Pascoli, Unravelling the richness of dark sector by FASERν, J. High Energy Phys. 10 (2020) 008.

[35] P. S. B. Dev, W. Rodejohann, X.-J. Xu, and Y. Zhang, MUonE sensitivity to new physics explanations of the muon anomalous magnetic moment, J. High Energy Phys. 05 (2020) 053.

[36] A. Masiero, P. Paradisi, and M. Passera, New physics at the MUonE experiment at CERN, Phys. Rev. D **102**, 075013 (2020).

[37] N. Nath, N. Okada, S. Okada, D. Raut, and Q. Shafi, Light Z' and Dirac fermion dark matter in the $B-L$ model, Eur. Phys. J. C **82**, 864 (2022).

[38] L. M. G. de la Vega, L. J. Flores, N. Nath, and E. Peinado, Complementarity between dark matter direct searches and CEνNS experiments in $U(1)'$ models, J. High Energy Phys. 09 (2021) 146.

[39] T. Araki, K. Asai, H. Otono, T. Shimomura, and Y. Takubo, Dark photon from light scalar boson decays at FASER, J. High Energy Phys. 03 (2021) 072; 06 (2021) 87.

[40] T. Felkl, T. Li, J. Liao, and M. A. Schmidt, Probing general $U(1)'$ models with non-universal lepton charges

at FASER/FASER2, COHERENT and long-baseline oscillation experiments, J. High Energy Phys. 09 (2023) 168.
[41] A. Elpe, E. Akyumuk, T. M. Aliev, L. Selbuz, and I. Turan, Constraining nonminimal dark sector scenarios with the COHERENT neutrino scattering data, Phys. Rev. D **107**, 075022 (2023).
[42] V. De Romeri, O. G. Miranda, D. K. Papoulias, G. Sanchez Garcia, M. Tórtola, and J. W. F. Valle, Physics implications of a combined analysis of COHERENT CsI and LAr data, J. High Energy Phys. 04 (2023) 035.
[43] P. Melas, D. K. Papoulias, and N. Saoulidou, Probing generalized neutrino interactions with DUNE near detector, J. High Energy Phys. 07 (2023) 190.
[44] FASER Collaboration, Technical proposal for FASER: Forward search experiment at the LHC, arXiv:1812.09139.
[45] FASER Collaboration, FASER: Forward search experiment at the LHC, arXiv:1901.04468.
[46] FASER Collaboration, First neutrino interaction candidates at the LHC, Phys. Rev. D **104**, L091101 (2021).
[47] FASER Collaboration, Detecting and studying high-energy collider neutrinos with FASER at the LHC, Eur. Phys. J. C **80**, 61 (2020).
[48] FASER Collaboration, Technical proposal: FASERnu, arXiv:2001.03073.
[49] C. A. Argüelles *et al.*, Snowmass white paper: Beyond the standard model effects on neutrino flavor, Eur. Phys. J. C **83**, 15 (2023).
[50] J. L. Feng *et al.*, The forward physics facility at the high-luminosity LHC, J. Phys. G **50**, 030501 (2023).
[51] FASER Collaboration, Measuring TeV neutrinos with FASERν in LHC run 3, *Proc. Sci.*, EPS-HEP2021 (2022) 248.
[52] G. Acampora *et al.*, SND@LHC—Scattering and neutrino detector at the LHC, CERN, Geneva, 2022.
[53] SHiP Collaboration, A facility to Search for Hidden Particles (SHiP) at the CERN SPS, arXiv:1504.04956.
[54] SND@LHC Collaboration, SND@LHC: The scattering and neutrino detector at the LHC, arXiv:2210.02784.
[55] SHiP Collaboration, SND@LHC, arXiv:2002.08722.
[56] NA64 Collaboration, Search for a new $B-L$ Z' gauge boson with the NA64 experiment at CERN, Phys. Rev. Lett. **129**, 161801 (2022).
[57] NA64 Collaboration, Search for invisible decays of sub-GeV dark photons in missing-energy events at the CERN SPS, Phys. Rev. Lett. **118**, 011802 (2017).
[58] NA64 Collaboration, Search for vector mediator of dark matter production in invisible decay mode, Phys. Rev. D **97**, 072002 (2018).
[59] D. Banerjee *et al.*, Dark matter search in missing energy events with NA64, Phys. Rev. Lett. **123**, 121801 (2019).
[60] S. N. Gninenko, N. V. Krasnikov, and V. A. Matveev, Search for dark sector physics with NA64, Phys. Part. Nucl. **51**, 829 (2020).
[61] H. Sieber, D. Banerjee, P. Crivelli, E. Depero, S. N. Gninenko, D. V. Kirpichnikov, M. M. Kirsanov, V. Poliakov, and L. Molina Bueno, Prospects in the search for a new light Z' boson with the NA64μ experiment at the CERN SPS, Phys. Rev. D **105**, 052006 (2022).
[62] G. Abbiendi, Letter of Intent: The MUonE project, Reports No. CERN-SPSC-2019-026, No. SPSC-I-252, CERN, Geneva, 2019.
[63] G. Abbiendi, Status of the MUonE experiment, Phys. Scr. **97**, 054007 (2022).
[64] M. Davier and H. Nguyen Ngoc, An unambiguous search for a light Higgs boson, Phys. Lett. B **229**, 150 (1989).
[65] NA64 Collaboration, Improved limits on a hypothetical $X(16.7)$ boson and a dark photon decaying into e^+e^- pairs, Phys. Rev. D **101**, 071101 (2020).
[66] G. A. Beer *et al.*, Emission of muonium into vacuum from a silica powder layer, Phys. Rev. Lett. **57**, 671 (1986).
[67] E. M. Riordan *et al.*, A search for short lived axions in an electron beam dump experiment, Phys. Rev. Lett. **59**, 755 (1987).
[68] J. D. Bjorken, S. Ecklund, W. R. Nelson, A. Abashian *et al.*, Search for neutral metastable penetrating particles produced in the SLAC beam dump, Phys. Rev. D **38**, 3375 (1988).
[69] A. Bross, M. Crisler, S. H. Pordes, J. Volk, S. Errede, and J. Wrbanek, A search for short-lived particles produced in an electron beam dump, Phys. Rev. Lett. **67**, 2942 (1991).
[70] TEXONO Collaboration, Measurement of $\bar{\nu}_e$-electron scattering cross-section with a CsI(Tl) scintillating crystal array at the Kuo-Sheng nuclear power reactor, Phys. Rev. D **81**, 072001 (2010).
[71] TEXONO Collaboration, Limit on the electron neutrino magnetic moment from the Kuo-Sheng reactor neutrino experiment, Phys. Rev. Lett. **90**, 131802 (2003).
[72] TEXONO Collaboration, A search of neutrino magnetic moments with a high-purity germanium detector at the Kuo-Sheng nuclear power station, Phys. Rev. D **75**, 012001 (2007).
[73] Borexino Collaboration, Science and technology of BOREXINO: A real time detector for low-energy solar neutrinos, Astropart. Phys. **16**, 205 (2002).
[74] G. Bellini *et al.*, Precision measurement of the ^{7}Be solar neutrino interaction rate in Borexino, Phys. Rev. Lett. **107**, 141302 (2011).
[75] B. T. Cleveland, T. Daily, R. Davis, Jr., J. R. Distel, K. Lande, C. K. Lee, P. S. Wildenhain, and J. Ullman, Measurement of the solar electron neutrino flux with the Homestake chlorine detector, Astrophys. J. **496**, 505 (1998).
[76] F. von Feilitzsch and N. Schmitz, The Homestake chlorine solar neutrino experiment: Past, present and future, Nucl. Phys. B, Proc. Suppl. **118**, 49 (2003).
[77] Borexino Collaboration, First real time detection of ^{7}Be solar neutrinos by Borexino, Phys. Lett. B **658**, 101 (2008).
[78] Borexino Collaboration, The Borexino detector at the Laboratori Nazionali del Gran Sasso, Nucl. Instrum. Methods Phys. Res., Sect. A **600**, 568 (2009).
[79] S. Ajimura *et al.*, Technical design report (TDR): Searching for a sterile neutrino at J-PARC MLF (E56, JSNS2), arXiv:1705.08629.
[80] CHARM-II Collaboration, An improved determination of the electroweak mixing angle from muon-neutrino electron scattering, Phys. Lett. B **259**, 499 (1991).

[81] CHARM-II Collaboration, A detector for the study of neutrino-electron scattering, Nucl. Instrum. Methods Phys. Res., Sect. A **278**, 670 (1989).

[82] CHARM-II Collaboration, Measurement of differential cross-sections for muon-neutrino electron scattering, Phys. Lett. B **302**, 351 (1993).

[83] CHARM-II Collaboration, Precision measurement of electroweak parameters from the scattering of muon-neutrinos on electrons, Phys. Lett. B **335**, 246 (1994).

[84] COHERENT Collaboration, COHERENT Collaboration data release from the first observation of coherent elastic neutrino-nucleus scattering, arXiv:1804.09459.

[85] M. Cadeddu, C. Giunti, Y. F. Li, and Y. Y. Zhang, Average CsI neutron density distribution from COHERENT data, Phys. Rev. Lett. **120**, 072501 (2018).

[86] M. Cadeddu, N. Cargioli, F. Dordei, C. Giunti, Y. F. Li, E. Picciau, and Y. Y. Zhang, Constraints on light vector mediators through coherent elastic neutrino nucleus scattering data from COHERENT, J. High Energy Phys. 01 (2021) 116.

[87] COHERENT Collaboration, First measurement of coherent elastic neutrino-nucleus scattering on argon, Phys. Rev. Lett. **126**, 012002 (2021).

[88] COHERENT Collaboration, COHERENT Collaboration data release from the first detection of coherent elastic neutrino-nucleus scattering on argon, arXiv:2006.12659.

[89] A. G. Beda, E. V. Demidova, D. V. Medvedev, M. V. Shirchenko, and A. S. Starostin, GEMMA experiment: Three years of the search for the neutrino magnetic moment, Phys. Part. Nucl. Lett. **7**, 406 (2010).

[90] A. Hayrapetyan *et al.* (CMS Collaboration), Search for direct production of GeV-scale resonances decaying to a pair of muons in proton-proton collisions at $\sqrt{s} = 13$ TeV, J. High Energy Phys. 12 (2023) 070.

[91] *BABAR* Collaboration, Search for a dark photon in e^+e^- collisions at *BABAR*, Phys. Rev. Lett. **113**, 201801 (2014).

[92] *BABAR* Collaboration, Search for invisible decays of a dark photon produced in e^+e^- collisions at *BABAR*, Phys. Rev. Lett. **119**, 131804 (2017).

[93] NOMAD Collaboration, Final NOMAD results on $\nu_\mu \to \nu_\tau$ and $\nu_e \to \nu_\tau$ oscillations including a new search for ν_τ appearance using hadronic τ decays, Nucl. Phys. **B611**, 3 (2001).

[94] CHARM Collaboration, Search for axion like particle production in 400-GeV proton-copper interactions, Phys. Lett. **157B**, 458 (1985).

[95] J. Blumlein and J. Brunner, New exclusion limits for dark gauge forces from beam-dump data, Phys. Lett. B **701**, 155 (2011).

[96] J. Blümlein and J. Brunner, New exclusion limits on dark gauge forces from proton Bremsstrahlung in beam-dump data, Phys. Lett. B **731**, 320 (2014).

[97] ALEPH, DELPHI, L3, OPAL, and LEP Electroweak Working Group Collaborations, A combination of preliminary electroweak measurements and constraints on the standard model, arXiv:hep-ex/0612034.

[98] ALEPH Collaboration, Study of the muon pair production at center-of-mass energies from 20-GeV to 136-GeV with the ALEPH detector, Phys. Lett. B **399**, 329 (1997).

[99] LEP Working Group for Higgs boson searches, ALEPH, DELPHI, L3, and OPAL Collaborations, Search for the Standard Model Higgs boson at LEP, Phys. Lett. B **565**, 61 (2003).

[100] ALEPH, DELPHI, L3, OPAL, SLD, LEP Electroweak Working Group, SLD Electroweak Group, and SLD Heavy Flavour Group Collaborations, Precision electroweak measurements on the Z resonance, Phys. Rep. **427**, 257 (2006).

[101] A. Davidson, BL as the fourth color within an $SU(2)_L \times U(1)_R \times U(1)$ model, Phys. Rev. D **20**, 776 (1979).

[102] A. Davidson, M. Koca, and K. C. Wali, $U(1)$ as the minimal horizontal gauge symmetry, Phys. Rev. Lett. **43**, 92 (1979).

[103] R. N. Mohapatra and R. E. Marshak, Local $B - L$ symmetry of electroweak interactions, Majorana neutrinos and neutron oscillations, Phys. Rev. Lett. **44**, 1316 (1980); **44**, 1643(E) (1980).

[104] C. Wetterich, Neutrino masses and the scale of $B - L$ violation, Nucl. Phys. **B187**, 343 (1981).

[105] A. Masiero, J. F. Nieves, and T. Yanagida, $B - L$ violating proton decay and late cosmological baryon production, Phys. Lett. **116B**, 11 (1982).

[106] W. Buchmuller, C. Greub, and P. Minkowski, Neutrino masses, neutral vector bosons and the scale of $B - L$ breaking, Phys. Lett. B **267**, 395 (1991).

[107] S. Jung, H. Murayama, A. Pierce, and J. D. Wells, Top quark forward-backward asymmetry from new t-channel physics, Phys. Rev. D **81**, 015004 (2010).

[108] T. Nomura and H. Okada, Minimal realization of right-handed gauge symmetry, Phys. Rev. D **97**, 015015 (2018).

[109] T. Nomura and H. Okada, Loop suppressed light fermion masses with $U(1)_R$ gauge symmetry, Phys. Rev. D **96**, 015016 (2017).

[110] S. Jana, P. K. Vishnu, and S. Saad, Minimal dirac neutrino mass models from $U(1)_{\mathrm{R}}$ gauge symmetry and left–right asymmetry at colliders, Eur. Phys. J. C **79**, 916 (2019).

[111] O. Seto and T. Shimomura, Atomki anomaly in gauged $U(1)_R$ symmetric model, J. High Energy Phys. 04 (2021) 025.

[112] J. C. Montero and V. Pleitez, Gauging U(1) symmetries and the number of right-handed neutrinos, Phys. Lett. B **675**, 64 (2009).

[113] E. Ma, Naturally small seesaw neutrino mass with no new physics beyond the TeV scale, Phys. Rev. Lett. **86**, 2502 (2001).

[114] CMS Collaboration, Search for resonant and nonresonant new phenomena in high-mass dilepton final states at $\sqrt{s} = 13$ TeV, J. High Energy Phys. 07 (2021) 208.

[115] ATLAS Collaboration, Search for high-mass dilepton resonances using 139 fb^{-1} of pp collision data collected at $\sqrt{s} = 13$ TeV with the ATLAS detector, Phys. Lett. B **796**, 68 (2019).

[116] F. Wang, W. Wang, and J. M. Yang, Split two-Higgs-doublet model and neutrino condensation, Europhys. Lett. **76**, 388 (2006).

[117] S. Gabriel and S. Nandi, A new two Higgs doublet model, Phys. Lett. B **655**, 141 (2007).

[118] S. M. Davidson and H. E. Logan, Dirac neutrinos from a second Higgs doublet, Phys. Rev. D **80**, 095008 (2009).

[119] N. Haba and M. Hirotsu, TeV-scale seesaw from a multi-Higgs model, Eur. Phys. J. C **69**, 481 (2010).
[120] F. Kling and L. J. Nevay, Forward neutrino fluxes at the LHC, Phys. Rev. D **104**, 113008 (2021).
[121] K. Kovarik *et al.*, nCTEQ15—Global analysis of nuclear parton distributions with uncertainties in the CTEQ framework, Phys. Rev. D **93**, 085037 (2016).
[122] A. Buckley, J. Ferrando, S. Lloyd, K. Nordström, Ben Page, Martin Rüfenacht, Marek Schönherr, and Graeme Watt, LHAPDF6: Parton density access in the LHC precision era, Eur. Phys. J. C **75**, 132 (2015).
[123] S. N. Gninenko, D. V. Kirpichnikov, M. M. Kirsanov, and N. V. Krasnikov, The exact tree-level calculation of the dark photon production in high-energy electron scattering at the CERN SPS, Phys. Lett. B **782**, 406 (2018).
[124] G. Abbiendi *et al.*, Measuring the leading hadronic contribution to the muon $g-2$ via μe scattering, Eur. Phys. J. C **77**, 139 (2017).
[125] G. Abbiendi, Letter of intent: The MUonE project, CERN, Report No. CERN-SPSC-2019-026, SPSC-I-252, 2019.
[126] C. M. Carloni Calame, M. Passera, L. Trentadue, and G. Venanzoni, A new approach to evaluate the leading hadronic corrections to the muon $g-2$, Phys. Lett. B **746**, 325 (2015).
[127] FASER Collaboration, First direct observation of collider neutrinos with FASER at the LHC, Phys. Rev. Lett. **131**, 031801 (2023).
[128] NA62 Collaboration, Search for dark photon decays to $\mu^+ \mu$ at NA62, J. High Energy Phys. 09 (2023) 035.
[129] A. G. Beda, V. B. Brudanin, V. G. Egorov, D. V. Medvedev *et al.*, Upper limit on the neutrino magnetic moment from three years of data from the GEMMA spectrometer, arXiv:1005.2736.
[130] COHERENT Collaboration, Measurement of the coherent elastic neutrino-nucleus scattering cross section on CsI by COHERENT, Phys. Rev. Lett. **129**, 081801 (2022).
[131] COHERENT Collaboration, Observation of coherent elastic neutrino-nucleus scattering, Science **357**, 1123 (2017).
[132] J. Barranco, O. G. Miranda, and T. I. Rashba, Probing new physics with coherent neutrino scattering off nuclei, J. High Energy Phys. 12 (2005) 021.
[133] K. Patton, J. Engel, G. C. McLaughlin, and N. Schunck, Neutrino-nucleus coherent scattering as a probe of neutron density distributions, Phys. Rev. C **86**, 024612 (2012).
[134] M. Cadeddu, F. Dordei, C. Giunti, Y. F. Li, E. Picciau, and Y. Y. Zhang, Physics results from the first COHERENT observation of coherent elastic neutrino-nucleus scattering in argon and their combination with cesium-iodide data, Phys. Rev. D **102**, 015030 (2020).
[135] J. Erler and S. Su, The weak neutral current, Prog. Part. Nucl. Phys. **71**, 119 (2013).
[136] R. H. Helm, Inelastic and elastic scattering of 187-MeV electrons from selected even-even nuclei, Phys. Rev. **104**, 1466 (1956).
[137] G. Fricke, C. Bernhardt, K. Heilig, L. A. Schaller, L. Schellenberg, E. B. Shera, and C. W. Dejager, Nuclear ground state charge radii from electromagnetic interactions, At. Data Nucl. Data Tables **60**, 177 (1995).
[138] I. Angeli and K. P. Marinova, Table of experimental nuclear ground state charge radii: An update, At. Data Nucl. Data Tables **99**, 69 (2013).
[139] M. Bender, K. Rutz, P. G. Reinhard, J. A. Maruhn, and W. Greiner, Shell structure of superheavy nuclei in self-consistent mean field models, Phys. Rev. C **60**, 034304 (1999).
[140] ALEPH, DELPHI, L3, OPAL, and LEP Electroweak Collaborations, Electroweak measurements in electron-positron collisions at W-boson-pair energies at LEP, Phys. Rep. **532**, 119 (2013).
[141] LHCb Collaboration, Search for $A' \to \mu^+\mu^-$ decays, Phys. Rev. Lett. **124**, 041801 (2020).
[142] A. Belyaev, N. D. Christensen, and A. Pukhov, CalcHEP 3.4 for collider physics within and beyond the standard model, Comput. Phys. Commun. **184**, 1729 (2013).
[143] F. Jegerlehner and A. Nyffeler, The muon $g-2$, Phys. Rep. **477**, 1 (2009).
[144] R. H. Parker, C. Yu, W. Zhong, B. Estey, and H. Müller, Measurement of the fine-structure constant as a test of the standard model, Science **360**, 191 (2018).
[145] L. Morel, Z. Yao, P. Cladé, and S. Guellati-Khélifa, Determination of the fine-structure constant with an accuracy of 81 parts per trillion, Nature (London) **588**, 61 (2020).
[146] Muon g-2 Collaboration, Measurement of the positive muon anomalous magnetic moment to 0.46 ppm, Phys. Rev. Lett. **126**, 141801 (2021).